THE UNIVERSITY of EDINBURGH

Edinburgh Research Explorer

Steady-state multiple near resonances of periodic interfacial waves with rigid boundary

Citation for published version:
Li, J, Liu, Z, Liao, S & Borthwick, AGL 2020, 'Steady-state multiple near resonances of periodic interfacial waves with rigid boundary', *Physics of Fluids*, vol. 32, no. 8, 087104. https://doi.org/10.1063/5.0015581

Digital Object Identifier (DOI):
10.1063/5.0015581

Link:
Link to publication record in Edinburgh Research Explorer

Document Version:
Peer reviewed version

Published In:
Physics of Fluids

General rights
Copyright for the publications made accessible via the Edinburgh Research Explorer is retained by the author(s) and / or other copyright owners and it is a condition of accessing these publications that users recognise and abide by the legal requirements associated with these rights.

Take down policy
The University of Edinburgh has made every reasonable effort to ensure that Edinburgh Research Explorer content complies with UK legislation. If you believe that the public display of this file breaches copyright please contact openaccess@ed.ac.uk providing details, and we will remove access to the work immediately and investigate your claim.

Download date: 19. Mar. 2025

Steady-state multiple near resonances of periodic interfacial waves with rigid boundary

Jiyang Li (李季阳),[1,a)] Zeng Liu (刘曾),[2,3,4,b)] Shijun Liao (廖世俊),[1,4,5,c)] and Alistair G. L. Borthwick[6,d)]

[1)] *School of Naval Architecture, Ocean and Civil Engineering, Shanghai Jiao Tong University, Shanghai 200240, China*

[2)] *School of Naval Architecture and Ocean Engineering, Huazhong University of Science and Technology, Wuhan 430074, China*

[3)] *Hubei Provincial Engineering Research Center of Data Techniques and Supporting Software for Ships, Wuhan, Hubei 430074, China*

[4)] *Collaborative Innovative Center for Advanced Ship and Deep-Sea Exploration, Shanghai 200240, China*

[5)] *State Key Laboratory of Ocean Engineering, Shanghai 200240, China*

[6)] *School of Engineering, University of Edinburgh, Edinburgh EH9 3FB, United Kingdom*

(Dated: 2 July 2020)

Steady-state resonant interfacial waves in a two-layer fluid within a frictionless duct is investigated theoretically. Solution procedure combined the homotopy analysis method (HAM) and Galerkin's method is used to search for accurate steady-state resonant solutions with multiple near resonances. In HAM, a piecewise parameter in the auxiliary linear operators is introduced to remove the small divisors caused by nearly resonant components. Convergent series solutions are then provided to the Galerkin iterations to accelerate the convergence rate. It is found that weakly nonlinear steady-state resonant waves form a continuum in the parameter space. As nonlinearity (wave steepness) increases, energy appears to be progressively shifted to sideband frequency components, effectively broadening the spectrum. The corresponding interfacial wave profile exhibits an almost fixed spatial pattern of repeated relatively high frequency, high amplitude bursts followed by low amplitude, longer waves. By examining the influence of density ratio, though changing slightly, the upper layer enlarges the amplitude of components near the primary ones while might reduces the amplitude of higher frequency components, enlarges the wave steepness and reduces the horizontal velocity of wave field. Our results indicate that steady-state systems with resonant interactions among periodic interfacial wave components could occur naturally in the oceans. All of this should enhance our understanding of periodic resonant interfacial waves.

[a] Electronic mail: lijiyang19930511@sjtu.edu.cn

[b] Author to whom correspondence should be addressed: z_liu@hust.edu.cn

[c] Electronic mail: sjliao@sjtu.edu.cn; homepage: http://sjliao.sjtu.edu.cn

[d] Electronic mail: Alistair.Borthwick@ed.ac.uk

I. INTRODUCTION

The subsea is a habitat for marine mammals, fish, plankton, and other organisms, and also provides the location and working environment for many man-made devices, including submarines, deep sea risers and elements of offshore structures. Autonomous underwater vehicles are nowadays routinely used for ocean exploration tasks including marine environmental monitoring, seabed mapping, and the mapping and exploitation of submarine resources (see e.g. Leonard *et al.* (1998); Leonard and Bahr (2016)). Internal waves commonly occur in the ocean owing to density stratification caused by temperature or salinity differences. They are believed to provide a transport mechanism for planktonic larvae and also to create so-called dead water zones which hinder ship propulsion.

Internal waves have been studied for decades (see e.g. Garrett and Munk (1979); Sutherland (2010); Dauxois *et al.* (2018)). Hunt (1961) derived a third-order approximation of progressive interfacial waves and considered the effect of upper fluid to the wave field. A general theoretical treatment of long internal waves, including solitary and periodic waves was proposed by Benjamin (1966, 1967). Holyer (1979) studied large amplitude, progressive interfacial waves moving between two infinite fluids of different densities. The Garrett-Munk internal wave spectrum accurately estimated internal wave energy spectra of most oceanic observations Garrett and Munk (1975). There have been many field observations of solitary internal waves. For example, Osborne and Burch (1980) reported observations of internal solitons in the Andaman Sea. In recent years, solitary internal waves (see e.g. Aghsaee, Boegman, and Lamb (2010); Grimshaw and Helfrich (2012)) and periodic internal waves (see e.g. Chen and Forbes (2008); Camassa *et al.* (2010)) have been further investigated through mathematical analysis, numerical simulation, and physical experiments. Although fewer studies have considered periodic internal waves than solitary internal waves owing to the practical difficulties encountered in conducting field observation campaigns and laboratory experiments, research into periodic internal waves is rather important, especially given that periodic progressive internal waves in layered fluids constitute a ‘well-documented phenomenon’ (see e.g. Holyer (1979); Saffman and Yuen (1982); Chen and Forbes (2008)).

Interactions among periodic waves can cause resonance, a topic that has been extensively researched in the context of surface gravity waves. The earliest study on surface wave resonance was undertaken by Phillips (1960) who derived the exact resonance criterion for a quartet of periodic progressive waves as

$$\boldsymbol{k}_1 \pm \boldsymbol{k}_2 \pm \boldsymbol{k}_3 \pm \boldsymbol{k}_4 = 0, \quad \omega_1 \pm \omega_2 \pm \omega_3 \pm \omega_4 = 0, \tag{1}$$

where $\boldsymbol{k}_i$ is the wave vector and ω_i is the associated linear angular frequency, with $i = 1, ..., 4$. Phillips (1960) found that the amplitude of the resonant wave component increases linearly with time. Another topic about resonant fluid flow is resonant gravity-driven films on wavy topographies. Linear and nonlinear resonance for viscous films on oblique wavy plane were studied by Wierschem *et al.* (2008) and Heining *et al.* (2009). Stabilities of film flows over topography were analyzed by Schörner, Reck, and Aksel (2015) and Aksel and Schörner (2018). Investigations into wave resonance have also extended to periodic internal gravity waves in continuous stratification and interfacial waves in discontinuous layered fluid. Studies of internal wave resonance include rate of energy transfer in the Garrett-Munk spectra (see e.g. Mccomas and Bretherton (1977)), collisions of internal wave beams in a uniformly stratified fluid (e.g. Akylas and Karimi (2012)), an instability mechanism causing resonant harmonic generation of internal gravity waves (see e.g. Liang, Zareei, and Alam (2017)), nearly resonant flow at the long-wavelength weakly nonlinear limit in a stratified fluid over topography (see e.g. Grimshaw and Smyth (1986); Zhang, King, and Swinney (2008)), etc. Studies of interfacial wave resonance in a two-layer fluid include Bragg resonance between surface-interfacial waves and a rippled bed (see e.g. Alam, Liu, and Yue (2009)), wave resonance between an 'internal' mode and an 'external' mode whose dispersion relation is the same as surface wave, each with the same phase speed but one having twice the wavelengths of the other (see e.g. Parau and Dias (2001)), and triad resonances among surface and interfacial waves (e.g. Ball (1964); Thorpe (1966); Wen (1995); Alam (2012); Tanaka and Wakayama (2015); Zaleski, Zaleski, and Lvov (2019)). To date, research into triad and higher-order interfacial wave resonances, including surface-interfacial waves and interfacial-interfacial waves, all concern wave systems with unsteady-state amplitudes which change slowly, or vary in the form of Jacobian elliptic functions, or have other relationships changing with time.

In recent years, in the field of surface gravity waves, by using the homotopy analysis method (HAM) (Liao (2003, 2011a); Vajravelu and Van Gorder (2012)), Liao (2011b) successfully overcame the problem of singularities identified by Madsen and Fuhrman (2012) and obtained single steady-state resonant quartet in deep water when condition (1) is exactly satisfied. Xu *et al.* (2012) and Liu and Liao (2014) then found that the steady-state resonant quartet could exist in water of finite depth and for more complicated cases. Similar results about the weakly nonlinear steady-state resonant quartet in water of finite depth have also been found from the Zakharov's equation (Xu *et al.*, 2012). In addition, using model basin tests, Liu *et al.* (2015) experimentally verified the existence of the surface wave systems discovered by Liao (2011b).

Although the foregoing theoretical analyses were based on an exact resonance criterion, there exist near-resonance criteria that are more generalized in their nature than the exact criterion. Without loss of generality, we consider a surface wave system with L nearly resonant components $(\boldsymbol{k}_{0,1}, \boldsymbol{k}_{0,2}, ..., \boldsymbol{k}_{0,L})$ that derived from two primary components $(\boldsymbol{k}_1, \boldsymbol{k}_2)$. It satisfies the following near-resonance criteria

$$m_l \boldsymbol{k}_1 + n_l \boldsymbol{k}_2 = \boldsymbol{k}_{0,l}, \quad m_l \omega_1 + n_l \omega_2 = \omega_{0,l} + d\omega_{0,l}, \quad l = 1, 2, ..., L, \tag{2}$$

where m_l and n_l are integers associated with the lth nearly resonant component, $\boldsymbol{k}_{0,l}$ is the wave vector, $\omega_{0,l}$ is the corresponding linear angular frequency, and $d\omega_{0,l}$ is the angular frequency mismatch (a small real number). Note that exact resonance can be regarded as a special case of near resonance, but with $d\omega_{0,i} = 0$. As Madsen and Fuhrman (2012) rightly pointed out, setting $d\omega_{0,i} = 0$ causes singularities, and inevitably setting $d\omega_{0,i} \approx 0$ for nearly resonant components would lead to very small denominators in the perturbation theory (see e.g. Liao, Xu, and Stiassnie (2016)). In the framework of the HAM, Liao, Xu, and Stiassnie (2016) developed an approach that successfully overcame this problem for single nearly resonant quartet when $L = 1$ in (2) and obtained solutions for steady-state surface gravity waves in deep water. Liu, Xu, and Liao (2017, 2018) and Liu and Xie (2019) extended the method to multiple near resonances when $L > 1$ in (2) and obtained finite amplitude steady-state surface wave systems in any arbitrary water depth. Meanwhile, steady-state resonant solutions for acoustic-gravity waves were also derived by Yang, Dias, and Liao (2018) using the HAM.

Unlike the unsteady-state system, there is no energy transfer between the various wave components in the steady-state resonant waves. In case of unsteady-state resonance, time-dependent periodic exchange of wave energy may happen and the nonlinear wave system would exhibit a Fermi-Pasta-Ulam recurrence phenomenon (Lake *et al.*, 1977). In case of steady-state resonance, amplitude of each component is invariant over the time. Therefore, the steady-state resonance represents an balanced state of wave energy and is a special case of the more general unsteady-state resonance, where the wave energy transfer among different wave components dynamically. Alam, Liu, and Yue (2010) pointed out that the dynamic evolution of wave spectrum with multiple resonances after a long time is complicated and intractable by traditional perturbation method. Steady-state resonance provides a way to study the evolution of complex wave system since the components in unsteady-state resonance are hard to be distinguished after long-term evolution with complicated wave generation and transformation. Besides, steady-state resonances could also be regarded as a benchmark to test the accuracy of any numerical algorithms for predicting the long-term evolution of wave systems. Knowledge of steady-state resonant systems provides insight into the behaviour of nonlinear interfacial wave evolution. To the authors' knowledge, a system containing resonant interactions among periodic interfacial gravity waves with time-independent amplitudes has not previously been identified.

The objective of this paper is to investigate steady-state resonant interfacial waves with rigid boundaries. A two-layer fluid within a frictionless duct of finite depth is considered. Assumption of a rigid top boundary holds for the following reason. Resonant interactions among the surface waves and the interface waves are quite complicated to since multiple external and internal modes of surface and interface waves have to been considered. When the depth of the upper fluid layer is sufficiently large, the influence of the surface on the interface can be ignored. Therefore, we consider a large depth of the upper fluid layer to simplify the problem to interface waves travelling under rigid top boundary. Physical parameters simplified from data in northeast of the South China Sea (NSCS) (21°N, 118.5°E) (Fan *et al.*, 2013) is used to simulate the real ocean environment. As a well-established analytical approximation method for nonlinear differential problems, especially in the field of steady-state resonant surface waves, the HAM is used in the present work to derive the steady-state resonant solutions of interfacial waves to certain level of accuracy. The resulting solutions are then taken as initial conditions for iteration in Galerkin's method (e.g. Okamura (2010); Liu and Xie (2019)) to obtain convergent solutions with enough accuracy.

The contributions of the current paper are summarized as follows. First, the existence of steady-state resonant interfacial waves is confirmed theoretically. It mainly extends the work of Hunt (1961) from progressive interfacial waves with single primary component to wave

FIG. 1. The physical sketch of the two-fluid system with related notations.

groups with two primary components that contains multiple resonances, and also extends the work of Liu and Xie (2019) from steady-state resonant surface waves to steady-state resonant interfacial waves. Second, accurate solutions of interfacial waves are obtained in circumstance near the real ocean environment. The influence of periodic interfacial wave groups on the underwater vehicle could be estimated. Lastly, effects of nonlinearity and density ratio on the physics of interfacial wave groups are analyzed. Continuum of the steady-state resonant interfacial waves in the parameter space is established. The current work aims to push forward the existence steady-state resonant waves to more general situations. We believe steady-state resonance happens for any kind of water waves if resonant interactions among different wave components appear.

The structure of this paper is as follows. § II outlines the mathematical derivation. § III presents results for linear resonance analysis, weakly nonlinear waves with single exactly resonant quartet, multiple nearly resonant waves with increased nonlinearity, and resonant waves with different density ratios. § IV summarizes the main conclusions.

II. MATHEMATICAL FORMULAE

A. Governing equations

Let us consider a system of two incompressible fluid layers each of constant density under gravity that entirely fill a frictionless duct. Following Alam (2012) and Tanaka and Wakayama (2015), it is assumed the flow is inviscid and irrotational inside each fluid layer. The inviscid model inevitably causes a discontinuity of shear stress around the interface. This drawback would be smeared out in practice and all analysis in this paper should still be useful. Fig. 1 illustrates the layered system for stable stratification density when $\rho_1 < \rho_2$. Here (x, y, z) represents the Cartesian coordinate system, in which $z = 0$ is a horizontal plane located at the undisturbed interface between the fluid layers and z is measured vertically upwards. The two-fluid system is bounded above and below by rigid surfaces located at $z = h_1$ and $z = -h_2$. The governing equations for each layer, kinematic boundary conditions, and kinematic and dynamic interface conditions are

$$\nabla^2\phi_1 = 0, \quad \zeta(x,y,t) < z < h_1, \tag{3}$$

$$\nabla^2\phi_2 = 0, \quad -h_2 < z < \zeta(x,y,t), \tag{4}$$

$$\frac{\partial\phi_1}{\partial z} = 0, \quad \text{at } z = h_1, \tag{5}$$

$$\frac{\partial\phi_2}{\partial z} = 0, \quad \text{at } z = -h_2, \tag{6}$$

$$\frac{\partial\zeta}{\partial t} + \nabla\phi_1\cdot\nabla\zeta - \frac{\partial\phi_1}{\partial z} = 0, \quad \text{at } z = \zeta(x,y,t), \tag{7}$$

$$\frac{\partial\zeta}{\partial t} + \nabla\phi_2\cdot\nabla\zeta - \frac{\partial\phi_2}{\partial z} = 0, \quad \text{at } z = \zeta(x,y,t), \tag{8}$$

$$\rho_1(\frac{\partial\phi_1}{\partial t} + g\zeta + \frac{1}{2}|\nabla\phi_1|^2) - \rho_2(\frac{\partial\phi_2}{\partial t} + g\zeta + \frac{1}{2}|\nabla\phi_2|^2) = 0, \quad \text{at } z = \zeta(x,y,t). \tag{9}$$

where $\phi_1(x,y,z,t)$ and $\phi_2(x,y,z,t)$ denote velocity potentials of the upper and lower fluid layers, $\zeta(x,y,t)$ is interfacial wave elevation, g is acceleration due to gravity, t is time, and $\nabla = \boldsymbol{i}\frac{\partial}{\partial x} + \boldsymbol{j}\frac{\partial}{\partial y} + \boldsymbol{k}\frac{\partial}{\partial z}$ is the gradient operator. For constant values of layer density,

$$\rho_1 = \rho_2\Delta, \quad 0 < \Delta < 1. \tag{10}$$

where Δ is density ratio. Consider a steady-state interfacial wave system with two primary periodic progressive waves. Let $\boldsymbol{k}_i$ denote the wave vector, σ_i the actual angular frequency and β_i the initial phase of the ith primary component. As amplitudes of all components in steady-state interfacial wave system are time-independent, we introduce the following transformation to search for steady-state solutions

$$\xi_i = \boldsymbol{k}_i\cdot\boldsymbol{r} - \sigma_i t + \beta_i, \quad i = 1,2, \tag{11}$$

where $\boldsymbol{r} = \boldsymbol{i}x + \boldsymbol{j}y$, and define

$$\varphi_1(\xi_1,\xi_2,z) = \phi_1(x,y,z,t), \;\; \varphi_2(\xi_1,\xi_2,z) = \phi_2(x,y,z,t), \;\; \eta(\xi_1,\xi_2) = \zeta(x,y,t) \tag{12}$$

in the new coordinate system (ξ_1,ξ_2,z). The original initial/boundary-value problem (3)-(9) in coordinate system (x,y,z,t) is then transformed into a boundary-value problem in coordinate system (ξ_1,ξ_2,z). Steady-state solutions can be more easily obtained from the boundary-value problem in coordinate system (ξ_1,ξ_2,z) and therefore the two coordinates

(ξ_1, ξ_2) play an important role in the rest of the analysis. The governing equations in coordinate system (ξ_1, ξ_2, z) read

$$\widehat{\nabla}^2 \varphi_1 = 0, \quad \eta(\xi_1, \xi_2) < z < h_1, \tag{13}$$

$$\widehat{\nabla}^2 \varphi_2 = 0, \quad -h_2 < z < \eta(\xi_1, \xi_2), \tag{14}$$

with three (two kinematic and one dynamic) boundary conditions at the unknown interface $z = \eta(\xi_1, \xi_2)$ (see appendix A for detailed derivation)

$$\begin{aligned} \mathcal{N}_1[\varphi_1, \varphi_2] = & \sum_{i=1}^{2} \sum_{j=1}^{2} \sigma_i \sigma_j \frac{\partial^2 \varphi_2}{\partial \xi_i \partial \xi_j} + g(1-\Delta) \frac{\partial \varphi_2}{\partial z} - \Delta \sum_{i=1}^{2} \sum_{j=1}^{2} \sigma_i \sigma_j \frac{\partial^2 \varphi_1}{\partial \xi_i \partial \xi_j} + \widehat{\nabla} \varphi_2 \cdot \widehat{\nabla} f_2 \\ & - 2 \sum_{i=1}^{2} \sigma_i \frac{\partial f_2}{\partial \xi_i} + \Delta (\sum_{i=1}^{2} \sigma_i \frac{\partial f_1}{\partial \xi_i} - h_{21} - \widehat{\nabla} \varphi_2 \cdot \widehat{\nabla} f_1) = 0, \end{aligned} \tag{15}$$

$$\begin{aligned} \mathcal{N}_2[\varphi_1, \varphi_2] = & \, g(1-\Delta) \frac{\partial (\varphi_2 - \varphi_1)}{\partial z} + \widehat{\nabla}(\varphi_2 - \varphi_1) \cdot \widehat{\nabla} f_2 - h_{12} - \sum_{i=1}^{2} \sigma_i \frac{\partial f_2}{\partial \xi_i} \\ & - \Delta [\sum_{i=1}^{2} \sigma_i \frac{\partial f_1}{\partial \xi_i} + h_{21} + \widehat{\nabla}(\varphi_2 - \varphi_1) \cdot \widehat{\nabla} f_1] = 0, \end{aligned} \tag{16}$$

$$\mathcal{N}_3[\varphi_1, \varphi_2, \eta] = \eta - \frac{1}{g(1-\Delta)} [\sum_{i=1}^{2} \sigma_i \frac{\partial \varphi_2}{\partial \xi_i} - f_2 - \Delta (\sum_{i=1}^{2} \sigma_i \frac{\partial \varphi_1}{\partial \xi_i} - f_1)] = 0, \tag{17}$$

and two boundary conditions at the upper and lower rigid surfaces

$$\frac{\partial \varphi_1}{\partial z} = 0, \quad \text{at } z = h_1, \tag{18}$$

$$\frac{\partial \varphi_2}{\partial z} = 0, \quad \text{at } z = -h_2, \tag{19}$$

where $\mathcal{N}_1$, $\mathcal{N}_2$ and $\mathcal{N}_3$ are nonlinear differential operators and

$$\widehat{\nabla} = \boldsymbol{k}_1 \frac{\partial}{\partial \xi_1} + \boldsymbol{k}_2 \frac{\partial}{\partial \xi_2} + \boldsymbol{k} \frac{\partial}{\partial z}, \quad f_i = \frac{1}{2} \left| \widehat{\nabla} \varphi_i \right|^2, \quad i = 1, 2, \tag{20}$$

$$h_{ij} = -\sigma_1 \widehat{\nabla} \varphi_i \cdot \widehat{\nabla} (\frac{\partial \varphi_j}{\partial \xi_1}) - \sigma_2 \widehat{\nabla} \varphi_i \cdot \widehat{\nabla} (\frac{\partial \varphi_j}{\partial \xi_2}), \quad i, j = 1, 2. \tag{21}$$

The interfacial wave elevation η and velocity potentials in the upper and lower fluid layers φ_i of steady-state interfacial wave system can be expressed in the form

$$\eta(\xi_1, \xi_2) = \sum_{i=-\infty}^{+\infty} \sum_{j=-\infty}^{+\infty} C_{i,j}^{\eta} \cos(i\xi_1 + j\xi_2), \tag{22}$$

$$\varphi_1(\xi_1, \xi_2, z) = \sum_{i=-\infty}^{+\infty} \sum_{j=-\infty}^{+\infty} C_{i,j}^{\varphi_1} \psi_{i,j}^1(\xi_1, \xi_2, z), \tag{23}$$

$$\varphi_2(\xi_1, \xi_2, z) = \sum_{i=-\infty}^{+\infty} \sum_{j=-\infty}^{+\infty} C_{i,j}^{\varphi_2} \psi_{i,j}^2(\xi_1, \xi_2, z), \tag{24}$$

where

$$\psi^1_{i,j}(\xi_1,\xi_2,z) = \cosh[|i\boldsymbol{k}_1 + j\boldsymbol{k}_2|\,(z-h_1)]\sin(i\xi_1 + j\xi_2), \tag{25}$$

$$\psi^2_{i,j}(\xi_1,\xi_2,z) = \cosh[|i\boldsymbol{k}_1 + j\boldsymbol{k}_2|\,(z+h_2)]\sin(i\xi_1 + j\xi_2). \tag{26}$$

Values of $\boldsymbol{k}_i$, σ_i and h_i with $i = 1, 2$ are given in each case to obtain the unknown constants $C^{\eta}_{i,j}$, $C^{\varphi_1}_{i,j}$ and $C^{\varphi_2}_{i,j}$. Equations (13)-(14) and (18)-(19) are automatically satisfied by the form of η, φ_i given by (22)-(24), and so the unknown constants are obtained by solving the three boundary conditions (15)-(17) at the internal interface $z = \eta(\xi_1, \xi_2)$.

B. Approach based on the HAM

General idea of the homotopy analysis method (HAM) is to construct a kind of continuous deformation between given solution (called initial guess) and the solution of the nonlinear differential equations to be solved. Detailed introduction of the HAM can be found in Liao (2003, 2011a); Vajravelu and Van Gorder (2012). Basic idea and important parts of the HAM are shown in this section.

Given that the expressions for φ_1 (23) and φ_2 (24) automatically satisfy the governing equations (13)-(14) and the top and bottom boundary conditions (18)-(19), it is sufficient solely to consider the interface conditions (15)-(17). We set $q \in [0, 1]$ as an embedding homotopy parameter, $c_0 \neq 0$ as a convergence-control parameter, $\mathcal{L}_1$ and $\mathcal{L}_2$ as the auxiliary linear operators, $\eta_0 = 0$ as initial approximation of interfacial wave elevation η and $\varphi_{0,1}(\xi_1, \xi_2, z)$ and $\varphi_{0,2}(\xi_1, \xi_2, z)$ as initial approximations of the potential functions φ_1 and φ_2. Then, based on the interface conditions (15)-(17), we construct the following parameterized family of equations (called the zeroth-order deformation equations):

$$(1-q)\mathcal{L}_1[\check{\varphi}_1 - \varphi_{0,1}, \check{\varphi}_2 - \varphi_{0,2}] = q c_0 \mathcal{N}_1[\check{\varphi}_1, \check{\varphi}_2], \quad \text{at } z = \check{\eta}, \tag{27}$$

$$(1-q)\mathcal{L}_2[\check{\varphi}_1 - \varphi_{0,1}, \check{\varphi}_2 - \varphi_{0,2}] = q c_0 \mathcal{N}_2[\check{\varphi}_1, \check{\varphi}_2], \quad \text{at } z = \check{\eta}, \tag{28}$$

$$(1-q)\check{\eta} = q c_0 \mathcal{N}_3[\check{\varphi}_1, \check{\varphi}_2, \check{\eta}], \quad \text{at } z = \check{\eta}, \tag{29}$$

where

$$\check{\varphi}_i(\xi_1, \xi_2, z; q) = \sum_{m=0}^{+\infty} \varphi_{m,i} q^m, \quad \varphi_{m,i}(\xi_1, \xi_2, z) = \frac{1}{m!}\frac{\partial^m \check{\varphi}_i}{\partial q^m}\bigg|_{q=0}, \quad i = 1, 2, \tag{30}$$

$$\check{\eta}(\xi_1, \xi_2; q) = \sum_{m=1}^{+\infty} \eta_m q^m, \quad \eta_m(\xi_1, \xi_2) = \frac{1}{m!} \frac{\partial^m \check{\eta}}{\partial q^m}\bigg|_{q=0}. \tag{31}$$

Considering the auxiliary linear operators $\mathcal{L}_1$ and $\mathcal{L}_2$ which have the property $\mathcal{L}_1[0,0] = \mathcal{L}_2[0,0] = 0$, we obtain the following relationships when $q = 0$:

$$\check{\varphi}_i(\xi_1, \xi_2, z; 0) = \varphi_{0,i}, \quad i = 1, 2, \quad \check{\eta}(\xi_1, \xi_2; 0) = 0, \tag{32}$$

When $q = 1$, equations (27)-(29) are equivalent to the original equations (15)-(17). Thus,

$$\check{\varphi}_i(\xi_1, \xi_2, z; 1) = \varphi_i, \quad i = 1, 2, \quad \check{\eta}(\xi_1, \xi_2; 1) = \eta, \tag{33}$$

So (27)-(29) define three homotopies:

$$\check{\varphi}_1 := \varphi_{0,1} \sim \varphi_1, \quad \check{\varphi}_2 := \varphi_{0,2} \sim \varphi_2, \quad \check{\eta} := 0 \sim \eta, \quad \text{when } q := 0 \sim 1, \tag{34}$$

Letting $q = 1$, the solutions for the interfacial wave elevation η and velocity potentials in the upper and lower fluid layer φ_i are approximated by

$$\varphi_i(\xi_1, \xi_2, z) = \check{\varphi}_i(\xi_1, \xi_2, z; 1) = \sum_{m=0}^{+\infty} \varphi_{m,i}(\xi_1, \xi_2, z), \quad i = 1, 2, \tag{35}$$

$$\eta(\xi_1, \xi_2) = \check{\eta}(\xi_1, \xi_2; 1) = \sum_{m=1}^{+\infty} \eta_m(\xi_1, \xi_2). \tag{36}$$

The sum index of interfacial wave elevation η starts from $m = 1$ as the initial guess $\eta_0 = 0$.

1. *Solution procedure*

The unknown $\varphi_{m,i}$ and η_m are governed by the high-order deformation equations

$$\overline{\mathcal{L}}_i[\varphi_{m,1}, \varphi_{m,2}] = c_0 \Delta^{\varphi}_{m-1,i} - \overline{S}_{m,i} + \chi_m S_{m-1,i}, \quad i = 1, 2, \tag{37}$$

$$\eta_m = c_0 \Delta^{\eta}_{m-1} + \chi_m \eta_{m-1}, \tag{38}$$

in which $\chi_1 = 0$ and $\chi_m = 1$ for $m \geq 2$, and $\overline{\mathcal{L}}_i = \mathcal{L}_i|_{z=0}$ are auxiliary linear operators.

Up to the mth order of approximation, all terms $\Delta^{\varphi}_{m-1,i}$, $\overline{S}_{m,i}$, $S_{m-1,i}$ and Δ^{η}_{m-1} on the right-hand side of the high-order deformation equations (37)-(38) are already predetermined by $\varphi_{n,i}$ and η_n, with $n = 0, 1, 2, ..., m-1$ and $m \geq 1$. Detailed expressions for $\Delta^{\varphi}_{m-1,i}$, $\overline{S}_{m,i}$, $S_{m-1,i}$ and Δ^{η}_{m-1} are given in appendix B and § II B 2. Note that η_m could be obtained directly from (38), meanwhile the solution process for $\varphi_{m,i}$ is more complicated.

When resonance conditions are nearly satisfied, proper auxiliary linear operators $\mathcal{L}_i$ must be chosen to remove the small divisors associated with near resonant components in $\varphi_{m,i}$. Otherwise, no convergent series solutions could be obtained for steady-state wave groups. This is why the perturbation method breaks down for steady-state wave groups when the resonance conditions are satisfied (Madsen and Fuhrman (2012)). Unlike the traditional perturbation method, the HAM does not depend on small physical parameters and instead provides freedom in the choices of auxiliary linear operator and initial guess. Convergent series solutions can therefore be obtained in the HAM framework for steady-state resonant wave groups.

2. Choice of auxiliary linear operators

Consider an interfacial wave system with L nearly resonant components $(\boldsymbol{k}_{0,1}, \boldsymbol{k}_{0,2}, ..., \boldsymbol{k}_{0,L})$ and two primary ones $(\boldsymbol{k}_1, \boldsymbol{k}_2)$. The resonance criteria are

$$i_l \boldsymbol{k}_1 + j_l \boldsymbol{k}_2 = \boldsymbol{k}_{0,l}, \quad i_l \omega_1 + j_l \omega_2 = \omega_{0,l} + d\omega_{0,l}, \quad l = 1, 2, \cdots, L, \tag{39}$$

where

$$\omega_i = \omega(k_i) = \sqrt{\frac{g k_i (1-\Delta) \tanh(k_i h_1) \tanh(k_i h_2)}{\tanh(k_i h_1) + \Delta \tanh(k_i h_2)}} \tag{40}$$

is the linear angular frequency with associated wave number $k_i = |\boldsymbol{k}_i|$. Here $d\omega_{0,l}$ is a small real number that represents the angular frequency mismatch of the lth resonant component.

For multiple resonances such as given by (39), the following auxiliary linear operators can be used to eliminate the small divisor caused by each nearly resonant component

$$\begin{aligned}\mathcal{L}_1[\varphi_1, \varphi_2] = {} & \omega_1^2 \frac{\partial^2 \varphi_2}{\partial \xi_1^2} + \mu \omega_1 \omega_2 \frac{\partial^2 \varphi_2}{\partial \xi_1 \partial \xi_2} + \omega_2^2 \frac{\partial^2 \varphi_2}{\partial \xi_2^2} + g(1-\Delta) \frac{\partial \varphi_2}{\partial z} \\ & - \Delta(\omega_1^2 \frac{\partial^2 \varphi_1}{\partial \xi_1^2} + \mu \omega_1 \omega_2 \frac{\partial^2 \varphi_1}{\partial \xi_1 \partial \xi_2} + \omega_2^2 \frac{\partial^2 \varphi_1}{\partial \xi_2^2}),\end{aligned} \tag{41}$$

$$\mathcal{L}_2[\varphi_1, \varphi_2] = g(1-\Delta)(\frac{\partial \varphi_2}{\partial z} - \frac{\partial \varphi_1}{\partial z}), \tag{42}$$

where

$$\mu(i,j) = \begin{cases} \frac{\omega^2(k_{i,j}) - (i^2\omega_1^2 + j^2\omega_2^2)}{ij\omega_1\omega_2}, & i = i_l, j = j_l \\ 2, & \text{else} \end{cases} \tag{43}$$

is a piecewise parameter depending on i and j in φ_i (23)-(24) and $k_{i,j} = |i\boldsymbol{k}_1 + j\boldsymbol{k}_2|$. This piecewise parameter is the key that eliminates the small divisors caused by all nearly resonant components and makes the HAM work. The auxiliary linear operators (41)-(42) are chosen based on the linear operators in boundary conditions (15)-(16). Expressions of $S_{m,i}$ and $\overline{S}_{m,i}$ can then be defined as

$$\begin{aligned} S_{m,1} &= \omega_1^2\beta_{2,0,2}^{m,0} + \mu\omega_1\omega_2\beta_{1,1,2}^{m,0} + \omega_2^2\beta_{0,2,2}^{m,0} + g(1-\Delta)\gamma_{0,0,2}^{m,0} \\ &\quad - \Delta(\omega_1^2\beta_{2,0,1}^{m,0} + \mu\omega_1\omega_2\beta_{1,1,1}^{m,0} + \omega_2^2\beta_{0,2,1}^{m,0}) + \overline{S}_{m,1}, \end{aligned} \tag{44}$$

$$\begin{aligned} \overline{S}_{m,1} &= \sum_{n=1}^{m-1}\left[\omega_1^2\beta_{2,0,2}^{m-n,n} + \mu\omega_1\omega_2\beta_{1,1,2}^{m-n,n} + \omega_2^2\beta_{0,2,2}^{m-n,n} + g(1-\Delta)\gamma_{0,0,2}^{m-n,n}\right. \\ &\quad \left. - \Delta(\omega_1^2\beta_{2,0,1}^{m-n,n} + \mu\omega_1\omega_2\beta_{1,1,1}^{m-n,n} + \omega_2^2\beta_{0,2,1}^{m-n,n})\right], \end{aligned} \tag{45}$$

$$\overline{S}_{m,2} = \sum_{n=1}^{m-1}\left[g(1-\Delta)(\gamma_{0,0,2}^{m-n,n} - \gamma_{0,0,1}^{m-n,n})\right], \tag{46}$$

$$S_{m,2} = g(1-\Delta)(\gamma_{0,0,2}^{m,0} - \gamma_{0,0,1}^{m,0}) + \overline{S}_{m,2}. \tag{47}$$

Detailed expressions of $\beta_{i,j,k}^{n,m}$ and $\gamma_{i,j,k}^{n,m}$ are shown in appendix B. Define the general form of $\varphi_{m,1}$ and $\varphi_{m,2}$ as

$$\varphi_{m,1} = \sum_{i,j} C_{i,j}^{\varphi_1,m}\psi_{i,j}^1, \quad \varphi_{m,2} = \sum_{i,j} C_{i,j}^{\varphi_2,m}\psi_{i,j}^2. \tag{48}$$

Then the mth-order deformation equations (37) can be simplified as

$$\overline{\mathcal{L}}_1[\sum_{i,j} C_{i,j}^{\varphi_1,m}\psi_{i,j}^1, \sum_{i,j} C_{i,j}^{\varphi_2,m}\psi_{i,j}^2] = \sum_{i,j} R_{i,j}^{1,m}\sin(i\xi_1 + j\xi_2), \tag{49}$$

$$\overline{\mathcal{L}}_2[\sum_{i,j} C_{i,j}^{\varphi_1,m}\psi_{i,j}^1, \sum_{i,j} C_{i,j}^{\varphi_2,m}\psi_{i,j}^2] = \sum_{i,j} R_{i,j}^{2,m}\sin(i\xi_1 + j\xi_2), \tag{50}$$

where $C_{i,j}^{\varphi_1,m}$ and $C_{i,j}^{\varphi_2,m}$ are constants to be determined for given $R_{i,j}^{1,m}$ and $R_{i,j}^{2,m}$. Equating the terms of both sides of equations (49)-(50), we obtain two linear algebraic equations

$$\begin{aligned} &\Delta(i^2\omega_1^2 + \mu ij\omega_1\omega_2 + j^2\omega_2^2)\cosh(k_{i,j}h_1)C_{i,j}^{\varphi_1,m} + [g(1-\Delta)k_{i,j}\sinh(k_{i,j}h_2) \\ &-(i^2\omega_1^2 + \mu ij\omega_1\omega_2 + j^2\omega_2^2)\cosh(k_{i,j}h_2)\big]\, C_{i,j}^{\varphi_2,m} = R_{i,j}^{1,m}, \end{aligned} \tag{51}$$

$$g(1-\Delta)k_{i,j}\left[\sinh(k_{i,j}h_1)C_{i,j}^{\varphi_1,m} + \sinh(k_{i,j}h_2)C_{i,j}^{\varphi_2,m}\right] = R_{i,j}^{2,m}. \tag{52}$$

The solutions for $C_{i,j}^{\varphi_1,m}$ and $C_{i,j}^{\varphi_2,m}$ are given by

$$C_{i,j}^{\varphi_1,m} = \frac{R_{i,j}^{2,m}}{g(1-\Delta)k_{i,j}\sinh(k_{i,j}h_1)} - \frac{\sinh(k_{i,j}h_2)}{\sinh(k_{i,j}h_1)}C_{i,j}^{\varphi_2,m}, \tag{53}$$

$$C_{i,j}^{\varphi_2,m} = \frac{A_{i,j}}{\lambda_{i,j}}\left(R_{i,j}^{1,m} - B_{i,j}R_{i,j}^{2,m}\right), \tag{54}$$

where

$$A_{i,j} = \frac{\tanh(k_{i,j}h_1)/\cosh(k_{i,j}h_2)}{\tanh(k_{i,j}h_1) + \Delta\tanh(k_{i,j}h_2)}, \tag{55}$$

$$B_{i,j} = \frac{\Delta(i^2\omega_1^2 + \mu ij\omega_1\omega_2 + j^2\omega_2^2)}{g(1-\Delta)k_{i,j}\tanh(k_{i,j}h_1)}, \tag{56}$$

$$\lambda_{i,j} = \omega^2(k_{i,j}) - (i^2\omega_1^2 + \mu ij\omega_1\omega_2 + j^2\omega_2^2). \tag{57}$$

For a non-resonant component $\cos(i\xi_1 + j\xi_2)$, $\mu(i,j) = 2$ and $\lambda_{i,j} = \omega^2(k_{i,j}) - (i\omega_1 + j\omega_2)^2$ is a non-small real number. $C_{i,j}^{\varphi_2,m}$ can be obtained directly from (54) and $C_{i,j}^{\varphi_1,m}$ is then computed from (53). For a nearly resonant component $\cos(i_l\xi_1 + j_l\xi_2)$, the value of $\mu(i_l, j_l)$ is determined so that it satisfies $\lambda_{i_l,j_l} = \omega^2(k_{i_l,j_l}) - (i_l^2\omega_1^2 + \mu i_l j_l\omega_1\omega_2 + j_l^2\omega_2^2) = 0$. Small divisor caused by nearly resonant component are changed into singularity associated with exact resonance. Since $\lambda_{i_l,j_l} = 0$ for nearly resonant component, $C_{i_l,j_l}^{\varphi_2,m}$ then cannot be obtained from (54) directly. To remove the singularity associated with resonance, we enforce the right-hand side of (54) equal to zero

$$R_{i_l,j_l}^{1,m} - \frac{\Delta\tanh(k_{i_l,j_l}h_2)}{\tanh(k_{i_l,j_l}h_1) + \Delta\tanh(k_{i_l,j_l}h_2)} R_{i_l,j_l}^{2,m} = 0, \tag{58}$$

from which the value of $C_{i_l,j_l}^{\varphi_2,m-1}$ is determined. Similarly, $C_{i_l,j_l}^{\varphi_2,m}$ is determined from the right-hand side of (54) via

$$R_{i_l,j_l}^{1,m+1} - \frac{\Delta\tanh(k_{i_l,j_l}h_2)}{\tanh(k_{i_l,j_l}h_1) + \Delta\tanh(k_{i_l,j_l}h_2)} R_{i_l,j_l}^{2,m+1} = 0. \tag{59}$$

It should be noted that for the two primary components $\cos(\xi_1)$ and $\cos(\xi_2)$, $\lambda_{1,0} = \lambda_{0,1} = 0$. Therefore, $C_{1,0}^{\varphi_2,m}$ and $C_{0,1}^{\varphi_2,m}$ are determined in a similar way as if the two primary components are resonant ones. Once the value of $C_{i,j}^{\varphi_2,m}$ is obtained, we can compute $C_{i,j}^{\varphi_1,m}$ directly from (53).

3. Choice of initial velocity potentials

Based on the linearized solutions of equations (15)-(17), we choose the following initial guesses

$$\begin{aligned} \varphi_{0,1} = &-\frac{\sinh(k_1h_2)}{\sinh(k_1h_1)} C_{1,0}^{\varphi_2,0}\psi_{1,0}^1 - \frac{\sinh(k_2h_2)}{\sinh(k_2h_1)} C_{0,1}^{\varphi_2,0}\psi_{0,1}^1 \\ &- \sum_{i=1}^{L} \frac{\sinh(k_{i_l,j_l}h_2)}{\sinh(k_{i_l,j_l}h_1)} C_{i_l,j_l}^{\varphi_2,0}\psi_{i_l,j_l}^1, \end{aligned} \tag{60}$$

$$\varphi_{0,2} = C_{1,0}^{\varphi_2,0}\psi_{1,0}^2 + C_{0,1}^{\varphi_2,0}\psi_{0,1}^2 + \sum_{l=1}^{L} C_{i_l,j_l}^{\varphi_2,0}\psi_{i_l,j_l}^2, \tag{61}$$

for velocity potentials and $\eta_0 = 0$ for interfacial wave elevation. Here the relationship between coefficients of $\psi^1_{i,j}$ and $\psi^2_{i,j}$ is derived directly from (53). When $m = 1$, equation (58) reduces to nonlinear algebraic equations, from which multiple solutions can be obtained for $C^{\varphi_2,0}_{i,j}$. When $m > 1$, equation (58) reduces to linear algebraic equations for $C^{\varphi_2,m-1}_{i,j}$. For weakly nonlinear waves, one resonant component in the initial guesses (60)-(61) ($L = 1$) is considered in order to obtain convergent steady-state solutions. As the nonlinearity (wave steepness) increases, wave energy increases and is more dispersed. Other components may join the resonance, so the number of resonant components (L) in the initial guess increase, too. A detailed example is given in § III C.

In the framework of HAM, proper auxiliary linear operator and initial guess are chosen to remove the small divisors associated with near resonance. Convergent series solutions could then be obtained successfully by symbolic arithmetic software such as Mathematica. Compared with the solution procedure of multiple steady-state resonances for surface waves (Liu, Xu, and Liao, 2018; Liu and Xie, 2019), the solution procedure for interfacial waves is more complicated. One more unknown velocity potential is considered in the kinematic and dynamic interface conditions. Besides, velocity potentials in the upper and lower fluid layers are coupled so they have to be solved simultaneously. The CUP time required for convergent series solution of steady-state resonant interfacial waves increases dramatically when either the order of approximation or the number of near resonant component in the initial guess increases. To accelerate the convergence rate of series solutions provided by HAM, we combine the HAM-based analytical approach and Galerkin method-based numerical approach. Once convergent series solutions of steady-state resonant interfacial waves have been found by HAM, the Galerkin method is used to obtain accurate steady-state solutions as the nonlinearity or density ratios changes.

C. Approach based on Galerkin's method

Based on the work of Okamura (2010) and Liu and Xie (2019), we express the interfacial wave elevation η and velocity potentials φ_i as

$$\eta(\xi_1,\xi_2) = \sum_{i=1}^{N}\sum_{j=-N}^{N} C_{i,j}^{\eta}\cos(i\xi_1 + j\xi_2) + \sum_{j=0}^{N} C_{0,j}^{\eta}\cos(j\xi_2), \tag{62}$$

$$\varphi_1(\xi_1,\xi_2,z) = \sum_{i=1}^{N}\sum_{j=-N}^{N} C_{i,j}^{\varphi_1}\psi_{i,j}^{1}(\xi_1,\xi_2,z) + \sum_{j=1}^{N} C_{0,j}^{\varphi_1}\psi_{0,j}^{1}(\xi_1,\xi_2,z), \tag{63}$$

$$\varphi_2(\xi_1,\xi_2,z) = \sum_{i=1}^{N}\sum_{j=-N}^{N} C_{i,j}^{\varphi_2}\psi_{i,j}^{2}(\xi_1,\xi_2,z) + \sum_{j=1}^{N} C_{0,j}^{\varphi_2}\psi_{0,j}^{2}(\xi_1,\xi_2,z). \tag{64}$$

with $6N(N+1)+1$ unknown coefficients ($C_{i,j}^{\eta}$, $C_{i,j}^{\varphi_1}$, and $C_{i,j}^{\varphi_2}$) to be determined.

After substituting (63)-(64) into (17), the discrete interface profile,

$$z = \eta(\xi_1,\xi_2) = \eta\left(\frac{2\pi(i-1)}{M}, \frac{2\pi(j-1)}{M}\right), \quad i,j = 1,2,...,M, \tag{65}$$

can be evaluated numerically by Newton's method for M^2 discrete points. Then substituting (65) into (15) and (16), we obtain

$$P_{r,s} = \int_0^{2\pi}\int_0^{2\pi} \mathcal{N}_1[\varphi_1,\varphi_2]\sin(r\xi_1 + s\xi_2)d\xi_1 d\xi_2 = 0, \quad \text{at } z = \eta(\xi_1,\xi_2), \tag{66}$$

$$Q_{r,s} = \int_0^{2\pi}\int_0^{2\pi} \mathcal{N}_2[\varphi_1,\varphi_2]\sin(r\xi_1 + s\xi_2)d\xi_1 d\xi_2 = 0, \quad \text{at } z = \eta(\xi_1,\xi_2), \tag{67}$$

which are calculated using M-point Fourier transforms. For $M > 2N+1$, $4N(N+1)$ independent equations can be obtained from (66) and (67) for $1 \le r \le N$, $-N \le s \le N$ and $1 \le s \le N$ with $r = 0$. The number of unknown coefficients $C_{i,j}^{\varphi_1}$ and $C_{i,j}^{\varphi_2}$ in the velocity potentials φ_1 and φ_2, $4N(N+1)$ equals the number of equations in (66) and (67). Hence, values of $C_{i,j}^{\varphi_1}$ and $C_{i,j}^{\varphi_2}$ can be computed by Newton's method. Finally, we substitute (63) and (64) into (17) and obtain

$$R_{r,s} = \int_0^{2\pi}\int_0^{2\pi} \mathcal{N}_3[\varphi_1,\varphi_2,\eta]\cos(r\xi_1 + s\xi_2)d\xi_1 d\xi_2 = 0, \quad \text{at } z = \eta(\xi_1,\xi_2), \tag{68}$$

which is evaluated by means of an M-point Fourier transform. For $M > 2N+1$, $2N(N+1)+1$ independent equations from (68) are obtained for $1 \le r \le N$, $-N \le s \le N$ and $0 \le s \le N$ with $r = 0$. The number of unknown coefficients $C_{i,j}^{\eta}$ in interfacial wave elevation η, $2N(N+1)$, equals the number of equations in (68), and so $C_{i,j}^{\eta}$ is also determined using Newton's

TABLE I. Dimensionless amplitude of dominant component $\left|C^{\eta}_{4,-3}\right| k_{4,-3}$ and wave steepness H_s in the form $(\left|C^{\eta}_{4,-3}\right| k_{4,-3}, H_s)$ of one solution for various values of N and M when $\Delta = 0.996$, $h_1/\lambda_2 = 0.5$, $h_2/\lambda_2 = 2$, $\alpha = \pi/36$, $k_2/k_1 = 0.895815$ and $\epsilon = 1.014$. α is the angle between the wave vectors of the two primary components and $\lambda_2 = 2\pi/k_2$. In the table — means divergent solutions.

$N\backslash M$	69	84	99
25	(0.11408,0.26575)	(0.11408,0.26576)	(0.11408,0.26576)
30	(0.11220,0.26591)	(0.11366,0.26543)	(0.11366,0.26543)
35	−−	(0.11376,0.26535)	(0.11375,0.26536)

method. When applying Galerkin's method, the initial solution is provided by the HAM and the iterations terminated once the maximum absolute difference between the unknown coefficients before and after an iteration reduces below 10^{-9}. Appendix C lists full details of the formulae used to evaluate the coefficients in the Jacobian matrices.

We define the dimensionless angular frequency $\epsilon = \sigma_1/\omega_1 = \sigma_2/\omega_2$ and the wave steepness

$$H_s = k_2 \frac{max[\eta(\xi_1,\xi_2)] - min[\eta(\xi_1,\xi_2)]}{2}, \quad \xi_1,\xi_2 \in [0, 2\pi]. \tag{69}$$

Here wave number of the second primary component k_2 is used as its value is fixed in different cases. Table I lists the dimensionless amplitude of the dominant component, $\left|C^{\eta}_{4,-3}\right| k_{4,-3}$ (only in this case), and the wave steepness, H_s, for different values of N and M when $\epsilon = 1.014$. It can be seen that the values of $\left|C^{\eta}_{4,-3}\right| k_{4,-3}$ and H_s remain unchanged for $M \geq 84$. The values of $\left|C^{\eta}_{4,-3}\right| k_{4,-3}$ and H_s converge as N increases from 25 to 35. Convergent solutions to four significant figures are obtained for this case where $N = 35$ and $M = 99$. In the other cases considered, convergence is to four significant figures.

III. RESULTS AND ANALYSIS

A. Linear resonance analysis

We first examine linear resonance in a duct. The geometric configuration and physical properties of the fluid layers are based on the following parameters for the north eastern

FIG. 2. (Colour online) The curves represent the location of the wave vector $\boldsymbol{k}_2$ (the second primary component) satisfying the resonance condition (39), once the wave vector $\boldsymbol{k}_1$ (the first primary component) is given in case of (70). The resonance curves stay quite close to each other, which suggests other components such as $2\boldsymbol{k}_1 - \boldsymbol{k}_2$ and $-\boldsymbol{k}_1 + 2\boldsymbol{k}_2$ may appear in the steady-state wave field while the second primary component move along the resonance curves.

FIG. 3. (Colour online) Relative angular frequency mismatch $\log_{10} \nu(m, n)$ versus wave number ratio k_2/k_1 in case of (70).

region of the South China Sea (NSCS) at (21°N, 118.5°E) (Fan *et al.*, 2013) :

$$\Delta = 0.996, \quad \frac{h_1}{\lambda_2} = 0.5, \quad \frac{h_2}{\lambda_2} = 2, \quad \alpha = \frac{\pi}{36}, \tag{70}$$

where α is the angle between the wave vectors of the two primary components $\boldsymbol{k}_1$ and $\boldsymbol{k}_2$, $\lambda_2 = 2\pi/k_2 = 1\ km$ is the wavelength of the second primary component (close to real internal waves in the ocean), h_1 is the depth of upper fluid layer, and h_2 is the depth of lower layer. We define the relative angular frequency mismatch as

$$\nu(m_l, n_l) = \frac{|d\omega_{0,l}|}{\omega_1}. \tag{71}$$

Fig. 2 shows the resonance curves of the second primary component $\boldsymbol{k}_2$ for given wave vector $\boldsymbol{k}_1$ of the first primary component. Here the resonance condition (39) is satisfied for any possible combination of the two primary components. It can be found that the resonance curves stay close to each other for any possible $\boldsymbol{k}_2$. Other components such as $2\boldsymbol{k}_1 - \boldsymbol{k}_2$ and $-\boldsymbol{k}_1 + 2\boldsymbol{k}_2$ may appear in the steady-state wave field due to resonant interactions.

Taking several possible nearly resonant components as an example, fig. 3 displays the dependence of relative angular frequency mismatch $\nu(m_l, n_l)$ on wave number ratio k_2/k_1. It can be seen that resonance occurs when k_2/k_1 is in the range $(0.84, 0.91)$. Here $k_2/k_1 = 0.895815$ is chosen so that the component $(2, -1)$ corresponds to exactly resonant one. Table II lists the 6 resonant components with smallest relative angular frequency mismatches $\log_{10} \nu(m_l, n_l)$. As the nonlinearity increases, these resonant components with small relative angular frequency mismatch may serve as possible candidates for inclusion in the initial guess (60)-(61).

TABLE II. 6 Near-resonant components with smallest relative angular frequency mismatches $\log_{10}\nu(m_l, n_l)$ in case of (70) and $k_2/k_1 = 0.895815$ for $|m| \le 20$ and $|n| \le 20$.

m_l	n_l	$\log_{10}\nu(m_l, n_l)$	m_l	n_l	$\log_{10}\nu(m_l, n_l)$
3	-2	-3.16	5	-4	-2.27
-1	2	-2.90	-2	3	-2.22
4	-3	-2.61	6	-5	-2.01

B. Weakly nonlinear waves with single exactly resonant quartet

Next, we consider weakly nonlinear interfacial wave systems for the case $\epsilon = 1.0002$ together with the parameters in (70). We consider the exactly resonant component $(2, -1)$ and two primary ones in the initial guesses (60)-(61). We define $L = 1$ in (39) and modify the auxiliary linear operator (41) accordingly. For $m = 1$, the nonlinear algebraic equations (58) governing $C_{1,0}^{\varphi_2,0}$, $C_{0,1}^{\varphi_2,0}$ and $C_{2,-1}^{\varphi_2,0}$ have three group of solutions, listed in Table V in appendix D, which we call S1, S2 and S3. Three group of solutions mean that three balanced states of wave energy exist for the weakly nonlinear cases considered here. It should be emphasised that number of weakly nonlinear solutions of interfacial waves with a steady-state quartet depends on the physical parameter considered in (70). Further calculations shows that the weakly nonlinear solutions of interfacial waves form a continuum in the parameter space. Therefore the number of weakly nonlinear solutions changes continuously from 3 to 0 when the physical parameters in (70) change. Similar phenomenon has also been found for weakly nonlinear surface waves by Liu and Liao (2014).

The interfacial wave energy of whole wave system may be defined approximately as

$$\Pi = \sum_{m=-\infty}^{+\infty} \sum_{n=-\infty}^{+\infty} (C_{m,n}^{\eta})^2. \tag{72}$$

Table III summarizes the energy distributions of the three convergent solutions. For weakly nonlinear waves, the total energy Π is mainly contained by the primary components and the exactly resonant component.

Then we consider the influence of density ratio on weakly nonlinear resonant waves. For (70) and $\epsilon = 1.0002$, we vary the density ratio Δ from 0 to 1. At the same time, the wave number ratio k_2/k_1 changes with Δ so that component $(2, -1)$ corresponds to exactly

TABLE III. Wave energy distributions and wave steepness H_s of weakly nonlinear steady-state resonant interfacial waves in case of (70) with $\epsilon = 1.0002$.

group	$\frac{(C^\eta_{1,0})^2}{\Pi}$ (%)	$\frac{(C^\eta_{0,1})^2}{\Pi}$ (%)	$\frac{(C^\eta_{2,-1})^2}{\Pi}$ (%)	$\frac{(C^\eta_{3,-2})^2}{\Pi}$ (%)	H_s
S1	40.80	50.07	8.813	0.3176	0.0313
S2	41.25	18.52	39.50	0.6580	0.0361
S3	9.800	11.94	78.19	0.0383	0.0351

FIG. 4. (Colour online) Wave amplitude $|C^\eta_{i,j} k_{i,j}|$ versus Δ with the parameters in (70) when $\epsilon = 1.0002$. Wave number ratio k_2/k_1 changes with Δ so that component $(2, -1)$ corresponds to exact resonance. Solid line, $|C^\eta_{1,0} k_{1,0}|$; dash-dotted line, $|C^\eta_{0,1} k_{0,1}|$; dashed line, $|C^\eta_{2,-1} k_{2,-1}|$.

resonant one. Fig. 4 shows the wave amplitude $|C^\eta_{i,j} k_{i,j}|$ of three solutions on Δ. It is found that as Δ increases, amplitude of each component increases continuously. That means the amplitude of each interfacial wave component tends to increases with the density ratio.

We define the average velocity along the interfacial wave profile in the upper and lower layer as

$$U_i = \frac{\int_0^{2\pi} \int_0^{2\pi} \sqrt{u_i^2 + v_i^2 + w_i^2}\Big|_{z=\eta} d\xi_1 d\xi_2}{4\pi^2 H_s \sqrt{g/k_2}}, \quad i = 1, 2 \tag{73}$$

where $(\boldsymbol{i}u_i, \boldsymbol{j}v_i, \boldsymbol{k}w_i) = \nabla\phi_i$. Fig. 5 shows the wave steepness H_s and average velocity U_i of three solutions on Δ. For all three solutions, the wave steepness H_s increases while the average velocity U_i decreases with Δ. For interfacial waves with larger density of upper layer, the wave steepness is higher than that of an interfacial waves with lighter upper layer, meanwhile the related average velocity is smaller than that of an interfacial waves with lighter upper layer. Existence of the upper layer enlarges the wave steepness while reduces the average velocity for weakly nonlinear interfacial wave systems.

FIG. 5. (Colour online) Wave steepness H_s and average velocity U_i versus Δ with the parameters in (70) when $\epsilon = 1.0002$. Wave number ratio k_2/k_1 changes with Δ so that component $(2, -1)$ corresponds to exact resonance. Solid line, S1; dash-dotted line, S2; dashed line, S3.

C. Multiple nearly resonant waves with increased nonlinearity

For wave components travelling in the same direction, the wave steepness increases with the dimensionless angular frequency ϵ. So in this section, the dimensionless angular frequency ϵ is increased to consider steady-state interfacial waves with multiple nearly resonances. In the HAM-based analytical approach, additional resonant components (refer to Table II) are considered in the initial guesses (60)-(61) when ϵ increases from 1.0002 to 1.008. Detailed components along with the associated coefficients in initial guess $\varphi_{0,2}$ (61) are shown in table V in appendix D. Once convergent series solution has been obtained by HAM for each case, the Galerkin iterations then continue based on the series solution to obtain more accurate results. For $\epsilon > 1.008$, we use the Galerkin method to obtain accurate steady-state solutions. Solutions with smaller ϵ is chosen as initial solution of the iteration for larger ϵ.

We define $\sigma(m,n) = m\sigma_1 + n\sigma_2$ as the actual angular frequency of component (m,n). Table IV lists the energy distributions of steady-state resonant interfacial waves for ϵ increased up to 1.0147. As ϵ increases, the summed energy proportion contained by two primary components occupies less than 10% of the total energy when $\epsilon \geq 1.004$. The energy proportions of lower frequency components (including $\sigma(2,-1)$, $\sigma(-1,2)$ and $\sigma(3,-2)$) appear to oscillate with ϵ, whereas the energy proportions of the lowest frequency components $\sigma(-2,3)$, $\sigma(-3,4)$ and almost all the remaining high frequency components increase monotonically. This indicates that energy is transferred from primary and part low frequency components to the lowest frequency components and high frequency components gradually, as the nonlinearity increases. Moreover, the dominant frequency shifts higher as ϵ increases, a finding that concurs with other surface gravity wave situations such as nonlinear sloshing in a rectangular tank where the angular frequency of nonlinear sloshing waves in shallow water increases with nonlinearity (see e.g. Tadjbakhsh and Keller (1960); Vanden-Broeck and Schwartz (1981); Tsai and Jeng (1994)).

Fig. 6 presents discrete frequency spectra of dimensionless amplitude $\left|C^{\eta}_{i,j} k_{i,j}\right|$, evaluated for six dimensionless angular frequencies ϵ in the range (1.0002, 1.0147). As ϵ increases, the maximum amplitudes $\left|C^{\eta}_{i,j} k_{i,j}\right|$ increase and many previously trivial components evolve into non-trivial ones that must not be neglected in the wave system. This means that increasing numbers of components participate in the resonance. The frequency band σ/σ_1 broadens as ϵ increases. Moreover, when the nonlinearity is weak ($\epsilon = 1.0002$), a single peak exists in the

TABLE IV. Energy distributions of steady-state multiple nearly resonant interfacial waves for different values of dimensionless angular frequency ϵ in group S2 in case of (70). In the table — means the wave component is small enough to be ignored.

energy distributions	dimensionless angular frequency ϵ								
	1.0002	1.002	1.004	1.006	1.008	1.01	1.012	1.014	1.0147
$(C^{\eta}_{1,0})^2/\Pi$ (%)	41.25	19.09	2.640	—	1.661	3.598	4.200	3.356	2.883
$(C^{\eta}_{0,1})^2/\Pi$ (%)	18.52	1.615	3.432	7.335	6.908	4.295	1.364	—	0.120
$(C^{\eta}_{2,-1})^2/\Pi$ (%)	39.50	42.39	32.81	18.34	7.040	1.217	—	0.772	0.815
$(C^{\eta}_{3,-2})^2/\Pi$ (%)	0.658	19.11	34.07	40.88	35.89	24.51	13.92	7.998	8.262
$(C^{\eta}_{-1,2})^2/\Pi$ (%)	—	15.00	18.12	9.701	3.668	0.378	0.578	4.188	6.711
$(C^{\eta}_{4,-3})^2/\Pi$ (%)	—	2.579	6.953	17.53	29.59	35.47	34.38	31.48	31.24
$(C^{\eta}_{5,-4})^2/\Pi$ (%)	—	0.120	—	0.822	5.541	13.84	20.75	23.06	19.66
$(C^{\eta}_{-2,3})^2/\Pi$ (%)	—	—	1.364	3.458	7.255	13.48	19.64	22.65	24.80
$(C^{\eta}_{6,-5})^2/\Pi$ (%)	—	—	0.345	0.668	—	0.630	2.732	3.389	1.591
$(C^{\eta}_{7,-6})^2/\Pi$ (%)	—	—	0.201	0.934	1.332	0.742	0.203	0.190	0.571
$(C^{\eta}_{8,-7})^2/\Pi$ (%)	—	—	—	0.249	0.811	1.129	0.967	0.772	0.475
$(C^{\eta}_{9,-8})^2/\Pi$ (%)	—	—	—	—	0.119	0.321	0.295	—	0.086
$(C^{\eta}_{-3,4})^2/\Pi$ (%)	—	—	—	—	0.092	0.322	0.815	1.362	1.408
$(C^{\eta}_{10,-9})^2/\Pi$ (%)	—	—	—	—	—	—	—	0.223	0.758
$(C^{\eta}_{11,-10})^2/\Pi$ (%)	—	—	—	—	—	—	0.072	0.362	0.503
$(C^{\eta}_{12,-11})^2/\Pi$ (%)	—	—	—	—	—	—	—	0.117	0.057

spectrum. However, when the nonlinearity is stronger, further local peaks appear (growing into sidebands at 4/5 and 3/2 of the primary frequency σ_1). Wave steepness H_s of group 2 increases to 0.28 for $\epsilon = 1.0147$.

Fig. 7 plots the interface elevation ζ profile over a distance of 20 km around the crests for three values of dimensionless angular frequency ϵ. The interface profiles exhibit alternating bursts of high frequency, high-amplitude narrow-banded waves followed by lower frequency, lower amplitude waves. Multiple waves of similar height exist in each high amplitude burst. There is a general growth in wave amplitude with increasing ϵ. For $\epsilon = 1.0147$, the maximum

FIG. 6. Discrete dimensionless amplitude spectra $\left|C^{\eta}_{i,j} k_{i,j}\right|$ for steady-state multiple nearly resonant interfacial waves for group S2 in case of (70).

FIG. 7. Spatial profiles of interfacial wave elevation ζ (m) at $t = 0$ s for group S2 in case of (70).

wave height of the calculated interfacial waves reaches 89 m and the wavelength of the wave group reaches near 8100 m. It is worth mentioning that the maximum wave height and wavelength of the steady-state resonant interface waves match with that of internal solitons in the Northeastern South China Sea (Ramp *et al.*, 2004). In practice, this would have implications for the movement of and stresses on a nuclear-powered submarine travelling at about 500 m below sea level.

To summarize, the foregoing has described solutions of steady-state periodic interfacial gravity waves with multiple resonances driven by nonlinearity (as exhibited by the interfacial wave energy spectra Fig. 6).

D. Resonant waves with different density ratios

We now examine the influence of density ratio on steady state near-resonant internal waves. Noting that the fluid densities above and below the interface of a Boussinesq wave are almost identical (Holyer (1979)), we approximate Boussinesq waves by setting $\Delta = 0.996$, and air-water interfacial waves by setting $\Delta = 0.001$. To examine the effect of changing the densities, two other density configurations $\Delta = 0.5$ and $\Delta = 0.1$ are studied here, keeping all other parameters the same.

Fig. 8 shows the discrete spectra of dimensionless amplitude $\left|C^{\eta}_{i,j} k_{i,j}\right|$ obtained for interfacial waves with four different density ratios for group S2 when $h_1/\lambda_2 = 0.5$, $h_2/\lambda_2 = 2$, $\alpha = \pi/36$ and $\epsilon = 1.012$. Here k_2/k_1 is determined so that the component $(2, -1)$ correspond-

FIG. 8. Discrete spectra of dimensionless amplitude $\left|C^{\eta}_{i,j} k_{i,j}\right|$ for different Δ for group S2 in case of $h_1/\lambda_2 = 0.5$, $h_2/\lambda_2 = 2$, $\alpha = \pi/36$ and $\epsilon = 1.012$. Wave number ratio k_2/k_1 changes with Δ so that component $(2, -1)$ corresponds to exact resonant one. (a): $\Delta = 0.001$; (b): $\Delta = 0.1$; (c): $\Delta = 0.5$; (d): $\Delta = 0.996$.

FIG. 9. Interface elevation ζ (m) profiles over a distance of 20 km about the main crests at $t = 0$ s for different Δ for group S2 in case of $h_1/\lambda_2 = 0.5$, $h_2/\lambda_2 = 2$, $\alpha = \pi/36$ and $\epsilon = 1.012$. Wave number ratio k_2/k_1 changes with Δ so that component $(2, -1)$ corresponds to exact resonance. (a): $\Delta = 0.001$; (b): $\Delta = 0.1$; (c): $\Delta = 0.5$; (d): $\Delta = 0.996$.

FIG. 10. (Colour online) Vertical profiles of $x-$ horizontal component of velocity at crests at $t = 0$ s for different Δ corresponding to solution S2 with $h_1/\lambda_2 = 0.5$, $h_2/\lambda_2 = 2$, $\alpha = \pi/36$ and $\epsilon = 1.012$. Wave number ratio k_2/k_1 changes with Δ so that component $(2, -1)$ corresponds to exact resonance. Solid line, $\Delta = 0.001$; dash-dotted line, $\Delta = 0.1$; dashed line, $\Delta = 0.5$; dotted line, $\Delta = 0.996$.

s to exact resonance for different values of Δ. It is found that the spectra of steady-state resonant interfacial waves change little with Δ. Amplitude of high frequency components near $\sigma/\sigma_1 \approx 2.3$ decreases while amplitude of components near the primary ones increases. Compared with the Boussinesq wave system, small part of energy is transferred to higher frequency components in the system of air-water interfacial waves. Though changing slightly, the upper layer enlarges the amplitude of components near the primary ones while might reduce the amplitude of higher frequency components.

Fig. 9 presents spatial profiles of the interface elevation ζ for interfacial waves of four different density ratios. Although the shapes of the interface profiles are similar, the maximum wave height increases with Δ. The wave steepness H_s reaches 0.15 and 0.23 for $\Delta = 0.001$ and 0.996, respectively. The upper layer enlarges the wave steepness of interfacial waves as the amplitude of components near the primary ones increases with the density ratio.

Fig. 10 displays vertical profiles of the horizontal $x-$ component of velocity for four density ratios. At the density interface, large velocity gradients occur for all four cases. The horizontal velocity of air-water interfacial waves ($\Delta = 0.001$) near the interface is far larger than that of the corresponding Boussinesq waves ($\Delta = 0.996$). In other words, the upper layer reduces the horizontal velocity of wave field. Although the inviscid model used in this paper inevitably causes a discontinuity in the horizontal velocity component, and this would be smeared out in practice, the foregoing interpretation should nevertheless be useful.

For progressive interfacial waves of finite amplitude, Hunt (1961) found that the principle effect of the upper fluid is to reduce the velocity of propagation and the amplitude of the higher harmonics in the wave profile. Here we might extend the conclusion of Hunt (1961) from the progressive waves with single primary component to more complicated wave groups with two primary components that contains multiple resonances. More calculations have been conducted for steady-state resonant interfacial waves in group S1 and S3 and similar conclusions about the effects of density ratio and nonlinearity could be obtained.

IV. CONCLUDING REMARKS

Using analytical HAM and numerical Galerkin's method, we have shown that steady-state periodic interfacial gravity wave solutions can exist under conditions of multiple near resonances for a two-layer fluid filling a frictionless duct with fixed upper and lower boundaries. To achieve this, the fully nonlinear governing equations are solved using the HAM to derive steady-state resonant solutions to certain level of accuracy and provide initial solutions that are then iterated using Galerkin's method to obtain convergent solutions with enough accuracy, according to multiple near resonance criteria. By inserting a piecewise parameter in the auxiliary linear operators and solving the high-order deformation equations simultaneously, the HAM was able to avoid arithmetic problems arising from small denominators and singularities (that affect the traditional perturbation method).

The physical parameters were chosen so that they approximate actual ocean conditions in the northeastern part of the South China Sea. In the spirit of previous studies by Liao (2011b), Liao, Xu, and Stiassnie (2016), Liu, Xu, and Liao (2018), and Yang, Dias, and Liao (2018), we believe that interfacial waves with time-independent spectra in the ocean may exhibit steady state resonance, in an analogous manner to surface gravity waves and acoustic-gravity waves. It should be noted that steady-state resonant surface waves (air-water interfacial waves) obtained by the HAM in previous studies are particular cases of the more general steady-state resonant interfacial waves considered in the present paper.

For weakly nonlinear interfacial waves with single exactly resonant quartet, three convergent solutions with different energy distributions are obtained for a system with two primary components and exactly resonant component. For the three solutions considered herein, energy related to these components dominates the total energy of the system. Analogous phenomena have previously been found in steady-state surface gravity waves with single resonant quartet by Liao (2011b), Xu *et al.* (2012), and Liao, Xu, and Stiassnie (2016). In addition, for all three solutions, the amplitude of each interfacial wave component tends to increases with the density ratio and the upper layer enlarges the wave steepness while reduces the average velocity. Here, the existence of steady-state periodic interfacial gravity waves with single exactly resonant quartet has been confirmed for the first time.

As nonlinearity increases, the interfacial wave energy spectrum broadens from a small primary peak to one with a larger primary peak and sideband peaks at frequencies that are 4/5 and 3/2 the primary wave frequency σ_1. The dominant frequency also exhibits a monotonic, though small, increase with nonlinearity. The spectra indicate that previously trivial components can become non-trivial as nonlinearity increases, and so cannot be neglected in the wave system as further components participate in resonance. At all levels of nonlinearity considered, the steady-state interfacial wave profile comprises two types of waves that appear in a repeating consecutive pattern: high (nearly constant) amplitude, high frequency waves followed by low (again nearly constant) amplitude, low frequency waves. Our results prove the theoretical existence of steady-state periodic interfacial gravity waves with multiple resonances.

We also confirm the existence of steady-state resonant interfacial waves with finite amplitude for other density ratios. It has been found that, though changing slightly, the upper layer might reduces the amplitude of high frequency components while increases the amplitude of components near the primary one. In addition, the upper layer increases the wave steepness of interfacial waves and decreases the horizontal velocity of wave field. The conclusion of Hunt (1961), which means the upper fluid reduces the velocity of propagation and the amplitude of the higher harmonics in the wave profile, might be extended from progressive waves with single primary component to more complicated wave groups with two primary components that contains multiple resonances.

In this work, depth of the upper fluid layer is sufficiently large so that we ignored the influence of the free surface on the interface. The interactions between the surface and interfacial waves in a shallower upper fluid layer will be considered in future. Besides, we considered steady-state resonant interfacial wave groups with discrete wave spectra. Extension from the discrete spectra to continuous spectra will also be considered.

ACKNOWLEDGMENT

This work was partly supported by the National Natural Science Foundation of China (approval no. 51609090 and approval nos. 11432009) and State Key Laboratory of Ocean Engineering of China (approval no. 1806).

DATA AVAILABILITY

The data that support the findings of this study are available form the corresponding author upon reasonable request.

Appendix A: Derivation of Interface conditions

The interface elevation ζ is obtained by solving equation (9) to give

$$\zeta = \frac{1}{g(\rho_2-\rho_1)}[\rho_1(\frac{\partial\phi_1}{\partial t}+\frac{1}{2}|\nabla\phi_1|^2)-\rho_2(\frac{\partial\phi_2}{\partial t}+\frac{1}{2}|\nabla\phi_2|^2)],\quad \text{at } z=\zeta, \tag{A1}$$

Carrying out partial differentiation of (A1) with respect to x, y, and t, and substituting into equations (7)-(8), ζ is then eliminated to give

$$\rho_2\frac{\partial^2\phi_2}{\partial t^2}+g(\rho_2-\rho_1)\frac{\partial\phi_2}{\partial z}-\rho_1\frac{\partial^2\phi_1}{\partial t^2}+\rho_2\frac{\partial(|\nabla\phi_2|^2)}{\partial t}-\rho_1\frac{\partial(\frac{1}{2}|\nabla\phi_1|^2)}{\partial t}$$
$$+\rho_2\nabla\phi_2\cdot\nabla(\frac{1}{2}|\nabla\phi_2|^2)-\rho_1\nabla\phi_2\cdot\nabla(\frac{\partial\phi_1}{\partial t}+\frac{1}{2}|\nabla\phi_1|^2)=0,\quad \text{at } z=\zeta, \tag{A2}$$

$$\rho_2\frac{\partial^2\phi_2}{\partial t^2}+g(\rho_2-\rho_1)\frac{\partial\phi_1}{\partial z}-\rho_1\frac{\partial^2\phi_1}{\partial t^2}-\rho_1\frac{\partial(|\nabla\phi_1|^2)}{\partial t}+\rho_2\frac{\partial(\frac{1}{2}|\nabla\phi_2|^2)}{\partial t}$$
$$-\rho_1\nabla\phi_1\cdot\nabla(\frac{1}{2}|\nabla\phi_1|^2)+\rho_2\nabla\phi_1\cdot\nabla(\frac{\partial\phi_2}{\partial t}+\frac{1}{2}|\nabla\phi_2|^2)=0,\quad \text{at } z=\zeta. \tag{A3}$$

Subtracting (A3) from (A2), we obtain

$$g(\rho_2-\rho_1)\frac{\partial(\phi_2-\phi_1)}{\partial z}+\sum_{i=1}^{2}\rho_i[\frac{\partial(\frac{1}{2}|\nabla\phi_i|^2)}{\partial t}+\nabla\phi_i\cdot\nabla(\frac{1}{2}|\nabla\phi_i|^2)]-\rho_1\nabla\phi_2\cdot\nabla(\frac{\partial\phi_1}{\partial t}$$
$$+\frac{1}{2}|\nabla\phi_1|^2)-\rho_2\nabla\phi_1\cdot\nabla(\frac{\partial\phi_2}{\partial t}+\frac{1}{2}|\nabla\phi_2|^2)=0,\quad \text{at } z=\zeta. \tag{A4}$$

Subsequent derivation is then based on the interface conditions (A1), (A2) and (A4). After transformation (11)-(12), the dynamic interface condition (A1) becomes

$$\mathcal{N}_3[\varphi_1,\varphi_2,\eta]=\eta-\frac{1}{g(1-\Delta)}[\sum_{i=1}^{2}\sigma_i\frac{\partial\varphi_2}{\partial\xi_i}-f_2-\Delta(\sum_{i=1}^{2}\sigma_i\frac{\partial\varphi_1}{\partial\xi_i}-f_1)]=0, \tag{A5}$$

the kinematic interface condition (A2) becomes

$$\mathcal{N}_1[\varphi_1,\varphi_2] = \sum_{i=1}^{2}\sum_{j=1}^{2}\sigma_i\sigma_j\frac{\partial^2\varphi_2}{\partial\xi_i\partial\xi_j} + g(1-\Delta)\frac{\partial\varphi_2}{\partial z} - \Delta\sum_{i=1}^{2}\sum_{j=1}^{2}\sigma_i\sigma_j\frac{\partial^2\varphi_1}{\partial\xi_i\partial\xi_j} + \widehat{\nabla}\varphi_2\cdot\widehat{\nabla}f_2$$
$$- 2\sum_{i=1}^{2}\sigma_i\frac{\partial f_2}{\partial\xi_i} + \Delta(\sum_{i=1}^{2}\sigma_i\frac{\partial f_1}{\partial\xi_i} - h_{21} - \widehat{\nabla}\varphi_2\cdot\widehat{\nabla}f_1) = 0, \tag{A6}$$

and another kinematic interface condition (A4) becomes

$$\mathcal{N}_2[\varphi_1,\varphi_2] = g(1-\Delta)\frac{\partial(\varphi_2-\varphi_1)}{\partial z} + \widehat{\nabla}(\varphi_2-\varphi_1)\cdot\widehat{\nabla}f_2 - h_{12} - \sum_{i=1}^{2}\sigma_i\frac{\partial f_2}{\partial\xi_i}$$
$$- \Delta[\sum_{i=1}^{2}\sigma_i\frac{\partial f_1}{\partial\xi_i} + h_{21} + \widehat{\nabla}(\varphi_2-\varphi_1)\cdot\widehat{\nabla}f_1] = 0. \tag{A7}$$

The three interface conditions (A5)-(A7) are all satisfied at the unknown interface $z = \eta(\xi_1,\xi_2)$.

Appendix B: Expressions of high-order deformation equations in HAM

Substituting the series (30)-(31) into the zeroth-order deformation equations (27)-(29) with $z = \check{\eta}$, then equating like powers of q, results in three linear equations (which we call the high-order deformation equations):

$$\overline{\mathcal{L}}_i[\varphi_{m,1},\varphi_{m,2}] = c_0\Delta^{\varphi}_{m-1,i} + \chi_m(S_{m-1,i} - \overline{S}_{m,i}),\quad i=1,2,\quad m\geq 1, \tag{B1}$$

$$\eta_m = c_0\Delta^{\eta}_{m-1} + \chi_m\eta_{m-1},\quad m\geq 1, \tag{B2}$$

in which

$$\Delta^{\varphi}_{m,1} = \sigma_1^2\bar{\phi}_m^{2,0,2} + 2\sigma_1\sigma_2\bar{\phi}_m^{1,1,2} + \sigma_2^2\bar{\phi}_m^{0,2,2} + g(1-\Delta)\bar{\phi}_{z,m}^{0,0,2}$$
$$- \Delta(\sigma_1^2\bar{\phi}_m^{2,0,1} + 2\sigma_1\sigma_2\bar{\phi}_m^{1,1,1} + \sigma_2^2\bar{\phi}_m^{0,2,1}) + \Lambda^{2,2}_{m,1}$$
$$- 2(\sigma_1\Gamma^2_{m,1} + \sigma_2\Gamma^2_{m,2}) + \Delta(\sigma_1\Gamma^1_{m,1} + \sigma_2\Gamma^1_{m,2} - \Lambda^{2,1}_{m,2} - \Lambda^{2,1}_{m,1}), \tag{B3}$$

$$\Delta^{\varphi}_{m,2} = g(1-\Delta)(\bar{\phi}_{z,m}^{0,0,2} - \bar{\phi}_{z,m}^{0,0,1}) - \sigma_1\Gamma^2_{m,1} - \sigma_2\Gamma^2_{m,2} + \Lambda^{2,2}_{m,1} - \Lambda^{1,2}_{m,2} - \Lambda^{1,2}_{m,1}$$
$$+ \Delta(\Lambda^{1,1}_{m,1} - \Lambda^{2,1}_{m,2} - \Lambda^{2,1}_{m,1} - \sigma_1\Gamma^1_{m,1} - \sigma_2\Gamma^1_{m,2}), \tag{B4}$$

$$\Delta^{\eta}_m = \eta_m + \frac{1}{g(1-\Delta)}[\Gamma^2_{m,0} - \sigma_1\bar{\phi}_m^{1,0,2} - \sigma_2\bar{\phi}_m^{0,1,2}$$
$$+ \Delta(\sigma_1\bar{\phi}_m^{1,0,1} + \sigma_2\bar{\phi}_m^{0,1,1} - \Gamma^1_{m,0})], \tag{B5}$$

in which

$$\Gamma^{k}_{m,0}=\sum_{n=0}^{m}(\frac{k_1^2}{2}\bar{\phi}^{1,0,k}_{n}\bar{\phi}^{1,0,k}_{m-n}+\boldsymbol{k}_1\cdot\boldsymbol{k}_2\bar{\phi}^{1,0,k}_{n}\bar{\phi}^{0,1,k}_{m-n}$$
$$+\frac{k_2^2}{2}\bar{\phi}^{0,1,k}_{n}\bar{\phi}^{0,1,k}_{m-n}+\frac{1}{2}\bar{\phi}^{0,0,k}_{z,n}\bar{\phi}^{0,0,k}_{z,m-n}),\quad k=1,2, \tag{B6}$$

$$\Gamma^{k}_{m,1}=\sum_{n=0}^{m}[k_1^2\bar{\phi}^{1,0,k}_{n}\bar{\phi}^{2,0,k}_{m-n}+\boldsymbol{k}_1\cdot\boldsymbol{k}_2(\bar{\phi}^{1,0,k}_{n}\bar{\phi}^{1,1,k}_{m-n}+\bar{\phi}^{2,0,k}_{n}\bar{\phi}^{0,1,k}_{m-n})$$
$$+k_2^2\bar{\phi}^{0,1,k}_{n}\bar{\phi}^{1,1,k}_{m-n}+\bar{\phi}^{0,0,k}_{z,n}\bar{\phi}^{1,0,k}_{z,m-n}],\quad k=1,2, \tag{B7}$$

$$\Gamma^{k}_{m,2}=\sum_{n=0}^{m}[k_1^2\bar{\phi}^{1,0,k}_{n}\bar{\phi}^{1,1,k}_{m-n}+\boldsymbol{k}_1\cdot\boldsymbol{k}_2(\bar{\phi}^{1,0,k}_{n}\bar{\phi}^{0,2,k}_{m-n}+\bar{\phi}^{0,1,k}_{n}\bar{\phi}^{1,1,k}_{m-n})$$
$$+k_2^2\bar{\phi}^{0,1,k}_{n}\bar{\phi}^{0,2,k}_{m-n}+\bar{\phi}^{0,0,k}_{z,n}\bar{\phi}^{0,1,k}_{z,m-n}],\quad k=1,2, \tag{B8}$$

$$\Gamma^{k}_{m,3}=\sum_{n=0}^{m}[k_1^2\bar{\phi}^{1,0,k}_{n}\bar{\phi}^{1,0,k}_{z,m-n}+\boldsymbol{k}_1\cdot\boldsymbol{k}_2(\bar{\phi}^{1,0,k}_{n}\bar{\phi}^{0,1,k}_{z,m-n}+\bar{\phi}^{0,1,k}_{n}\bar{\phi}^{1,0,k}_{z,m-n})$$
$$+k_2^2\bar{\phi}^{0,1,k}_{n}\bar{\phi}^{0,1,k}_{z,m-n}+\bar{\phi}^{0,0,k}_{z,n}\bar{\phi}^{0,0,k}_{zz,m-n}],\quad k=1,2, \tag{B9}$$

$$\Lambda^{i,j}_{m,1}=\sum_{n=0}^{m}[k_1^2\bar{\phi}^{1,0,i}_{n}\Gamma^{j}_{m-n,1}+\boldsymbol{k}_1\cdot\boldsymbol{k}_2(\bar{\phi}^{1,0,i}_{n}\Gamma^{j}_{m-n,2}+\bar{\phi}^{0,1,i}_{n}\Gamma^{j}_{m-n,1})$$
$$+k_2^2\bar{\phi}^{0,1,i}_{n}\Gamma^{j}_{m-n,2}+\bar{\phi}^{0,0,i}_{z,n}\Gamma^{j}_{m-n,3}],\quad i,j=1,2, \tag{B10}$$

$$\Lambda^{i,j}_{m,2}=-\sigma_1\sum_{n=0}^{m}[k_1^2\bar{\phi}^{1,0,i}_{n}\bar{\phi}^{2,0,j}_{m-n}+\boldsymbol{k}_1\cdot\boldsymbol{k}_2(\bar{\phi}^{1,0,i}_{n}\bar{\phi}^{1,1,j}_{m-n}+\bar{\phi}^{0,1,i}_{n}\bar{\phi}^{2,0,j}_{m-n})$$
$$+k_2^2\bar{\phi}^{0,1,i}_{n}\bar{\phi}^{1,1,j}_{m-n}+\bar{\phi}^{0,0,i}_{z,n}\bar{\phi}^{1,0,j}_{z,m-n}]-\sigma_2\sum_{n=0}^{m}[k_1^2\bar{\phi}^{1,0,i}_{n}\bar{\phi}^{1,1,j}_{m-n}+k_2^2\bar{\phi}^{0,1,i}_{n}\bar{\phi}^{0,2,j}_{m-n}$$
$$+\bar{\phi}^{0,0,i}_{z,n}\bar{\phi}^{0,1,j}_{z,m-n}+\boldsymbol{k}_1\cdot\boldsymbol{k}_2(\bar{\phi}^{1,0,i}_{n}\bar{\phi}^{0,2,j}_{m-n}+\bar{\phi}^{0,1,i}_{n}\bar{\phi}^{1,1,j}_{m-n})],\quad i,j=1,2, \tag{B11}$$

$$\mu_{m,n}=\begin{cases}\eta_n,\quad m=1,\quad n\geq 1,\\ \displaystyle\sum_{i=m-1}^{n-1}\mu_{m-1,i}\eta_{n-i},\quad m\geq 2,\quad n\geq m,\end{cases} \tag{B12}$$

$$\psi^{n,m}_{i,j,k}=\frac{\partial^{i+j}}{\partial\xi_1^i\partial\xi_2^j}\left(\frac{1}{m!}\frac{\partial^m\varphi_{n,k}}{\partial z^m}\bigg|_{z=0}\right),\quad k=1,2, \tag{B13}$$

$$\beta_{i,j,k}^{n,m} = \begin{cases} \psi_{i,j,k}^{n,0}, & m = 0, \\ \sum_{s=1}^{m} \psi_{i,j,k}^{n,s} \mu_{s,m}, & m \geq 1, \end{cases} \tag{B14}$$

$$\gamma_{i,j,k}^{n,m} = \begin{cases} \psi_{i,j,k}^{n,1}, & m = 0, \\ \sum_{s=1}^{m} (s+1) \psi_{i,j,k}^{n,s+1} \mu_{s,m}, & m \geq 1, \end{cases} \tag{B15}$$

$$\delta_{i,j,k}^{n,m} = \begin{cases} 2\psi_{i,j,k}^{n,2}, & m = 0, \\ \sum_{s=1}^{m} (s+1)(s+2) \psi_{i,j,k}^{n,s+2} \mu_{s,m}, & m \geq 1, \end{cases} \tag{B16}$$

$$\bar{\phi}_n^{i,j,k} = \sum_{m=0}^{n} \beta_{i,j,k}^{n-m,m}, \quad \bar{\phi}_{z,n}^{i,j,k} = \sum_{m=0}^{n} \gamma_{i,j,k}^{n-m,m}, \quad \bar{\phi}_{zz,n}^{i,j,k} = \sum_{m=0}^{n} \delta_{i,j,k}^{n-m,m}. \tag{B17}$$

The linear operators are prescribed such that $\overline{\mathcal{L}}_1 = \mathcal{L}_1|_{z=0}$ and $\overline{\mathcal{L}}_2 = \mathcal{L}_2|_{z=0}$. Expressions for $\mathcal{L}_i$, $S_{m-1,i}$ and $\overline{S}_{m,i}$, with $i = 1, 2$, are given in § II B 2.

Appendix C: Detailed derivation of the Jacobian matrixes

The Jacobian matrixes, including $\partial P_{r,s}/\partial C_{i,j}^{\varphi_1}$, $\partial P_{r,s}/\partial C_{i,j}^{\varphi_2}$, $\partial Q_{r,s}/\partial C_{i,j}^{\varphi_1}$, $\partial Q_{r,s}/\partial C_{i,j}^{\varphi_2}$ and $\partial R_{r,s}/\partial C_{i,j}^{\eta}$, are given by

$$\frac{\partial P_{r,s}}{\partial C_{i,j}^{\varphi_1}} = \int_0^{2\pi} \int_0^{2\pi} \left(\frac{\partial \mathcal{N}_1}{\partial C_{i,j}^{\varphi_1}} + \frac{\partial \mathcal{N}_1}{\partial z} \frac{\partial \eta}{\partial C_{i,j}^{\varphi_1}}\right) \sin(r\xi_1 + s\xi_2) d\xi_1 d\xi_2, \tag{C1}$$

$$\frac{\partial P_{r,s}}{\partial C_{i,j}^{\varphi_2}} = \int_0^{2\pi} \int_0^{2\pi} \left(\frac{\partial \mathcal{N}_1}{\partial C_{i,j}^{\varphi_2}} + \frac{\partial \mathcal{N}_1}{\partial z} \frac{\partial \eta}{\partial C_{i,j}^{\varphi_2}}\right) \sin(r\xi_1 + s\xi_2) d\xi_1 d\xi_2, \tag{C2}$$

$$\frac{\partial Q_{r,s}}{\partial C_{i,j}^{\varphi_1}} = \int_0^{2\pi} \int_0^{2\pi} \left(\frac{\partial \mathcal{N}_2}{\partial C_{i,j}^{\varphi_1}} + \frac{\partial \mathcal{N}_2}{\partial z} \frac{\partial \eta}{\partial C_{i,j}^{\varphi_1}}\right) \sin(r\xi_1 + s\xi_2) d\xi_1 d\xi_2, \tag{C3}$$

$$\frac{\partial Q_{r,s}}{\partial C_{i,j}^{\varphi_2}} = \int_0^{2\pi} \int_0^{2\pi} \left(\frac{\partial \mathcal{N}_2}{\partial C_{i,j}^{\varphi_2}} + \frac{\partial \mathcal{N}_2}{\partial z} \frac{\partial \eta}{\partial C_{i,j}^{\varphi_2}}\right) \sin(r\xi_1 + s\xi_2) d\xi_1 d\xi_2, \tag{C4}$$

$$\frac{\partial R_{r,s}}{\partial C_{i,j}^{\eta}} = \int_0^{2\pi} \int_0^{2\pi} \frac{\partial \mathcal{N}_3[\varphi_1, \varphi_2, z]}{\partial z} \cos(i\xi_1 + j\xi_2) \cos(r\xi_1 + s\xi_2) d\xi_1 d\xi_2, \tag{C5}$$

where the unknowns $\partial\eta/\partial C^{\varphi_1}_{i,j}$ and $\partial\eta/\partial C^{\varphi_2}_{i,j}$ are determined by the equations

$$\frac{\partial\mathcal{N}_3[\varphi_1,\varphi_2,z]}{\partial C^{\varphi_1}_{i,j}}+\frac{\partial\mathcal{N}_3[\varphi_1,\varphi_2,z]}{\partial z}\frac{\partial\eta}{\partial C^{\varphi_1}_{i,j}}=0, \tag{C6}$$

$$\frac{\partial\mathcal{N}_3[\varphi_1,\varphi_2,z]}{\partial C^{\varphi_2}_{i,j}}+\frac{\partial\mathcal{N}_3[\varphi_1,\varphi_2,z]}{\partial z}\frac{\partial\eta}{\partial C^{\varphi_2}_{i,j}}=0. \tag{C7}$$

from (17). The expressions for $\mathcal{N}_1$, $\mathcal{N}_2$ and $\mathcal{N}_3$ are as follows:

$$\begin{aligned}\mathcal{N}_1[\varphi_1,\varphi_2]=&\,{TF_2}^2\varphi_{2\xi_1\xi_1}+2TF_2TS_2\varphi_{2\xi_1\xi_2}+{TS_2}^2\varphi_{2\xi_2\xi_2}+\varphi_{2z}[2TF_2\varphi_{2\xi_1z}\\&+2TS_2\varphi_{2\xi_2z}+g(1-\Delta)+\varphi_{2z}\varphi_{2zz}]-\Delta[TF_2TF_1\varphi_{1\xi_1\xi_1}+(TS_1TF_2\\&+TF_1TS_2)\varphi_{1\xi_1\xi_2}+TS_2TS_1\varphi_{1\xi_2\xi_2}+(TF_1\varphi_{2z}+TF_2\varphi_{1z})\varphi_{1\xi_1z}\\&+(TS_1\varphi_{2z}+TS_2\varphi_{1z})\varphi_{1\xi_2z}+\varphi_{2z}\varphi_{1z}\varphi_{1zz}],\end{aligned} \tag{C8}$$

$$\begin{aligned}\mathcal{N}_2[\varphi_1,\varphi_2]=&\,[g(1-\Delta)+\varphi_{2z}\varphi_{2zz}]DP_z+TF_2DTF\varphi_{2\xi_1\xi_1}+(TS_2DTF+TF_2DTS)\varphi_{2\xi_1\xi_2}\\&+TS_2DTS\varphi_{2\xi_2\xi_2}+(DTF\varphi_{2z}+TF_2DP_z)\varphi_{2\xi_1z}+(DTS\varphi_{2z}\\&+TS_2DP_z)\varphi_{2\xi_2z}-\Delta[TF_1DTF\varphi_{1\xi_1\xi_1}+(TS_1DTF\\&+TF_1DTS)\varphi_{1\xi_1\xi_2}+TS_1DTS\varphi_{1\xi_2\xi_2}+(DTF\varphi_{1z}+TF_1DP_z)\varphi_{1\xi_1z}\\&+(DTS\varphi_{1z}+TS_1DP_z)\varphi_{1\xi_2z}+\varphi_{1z}\varphi_{1zz}DP_z],\end{aligned} \tag{C9}$$

$$\begin{aligned}\mathcal{N}_3[\varphi_1,\varphi_2,z]=&\,z-\frac{1}{2g(1-\Delta)}\{(\sigma_1-TF_2)\varphi_{2\xi_1}+(\sigma_2-TS_2)\varphi_{2\xi_2}-\varphi^2_{2z}\\&-\Delta[(\sigma_1-TF_1)\varphi_{1\xi_1}+(\sigma_2-TS_1)\varphi_{1\xi_2}-\varphi^2_{1z}]\},\end{aligned} \tag{C10}$$

where

$$TF_j=k_1^2\varphi_{j\xi_1}+\boldsymbol{k}_1\cdot\boldsymbol{k}_2\varphi_{j\xi_2}-\sigma_1,\ TS_j=k_2^2\varphi_{j\xi_2}+\boldsymbol{k}_1\cdot\boldsymbol{k}_2\varphi_{j\xi_1}-\sigma_2,\ j=1,2, \tag{C11}$$

$$DTF=TF_2-TF_1,\ DTS=TS_2-TS_1,\ DP_z=\varphi_{2z}-\varphi_{1z}. \tag{C12}$$

Formulae for $\partial\mathcal{N}_r/\partial C^{\varphi_1}_{i,j}$, $\partial\mathcal{N}_r/\partial C^{\varphi_2}_{i,j}$ and $\partial\mathcal{N}_r/\partial z$, with $r=1,2,3$, are obtained by direct derivation.

Appendix D: Detailed results of initial guess in HAM

In § III B, when $m=1$, nonlinear algebraic equations (58) about $C^{\varphi_2,0}_{1,0}$, $C^{\varphi_2,0}_{0,1}$ and $C^{\varphi_2,0}_{2,-1}$ have three group of solutions, as listed in Table V.

In § III C, the detailed components together with absolute values of the associated coefficients in the initial guess $\varphi_{0,2}$ (61) for group S2 in case of (70) are shown in Table VI.

TABLE V. The solutions of the nonlinear algebraic equations (58) in case of (70) with $\epsilon = 1.0002$.

group	$\left\|C_{1,0}^{\varphi_2,0}\right\|$ (m^2/s)	$\left\|C_{0,1}^{\varphi_2,0}\right\|$ (m^2/s)	$\left\|C_{2,-1}^{\varphi_2,0}\right\|$ (m^2/s)
S1	3.66×10^{-6}	2.76×10^{-5}	3.96×10^{-7}
S2	3.45×10^{-6}	1.35×10^{-5}	5.39×10^{-7}
S3	3.25×10^{-6}	1.05×10^{-5}	1.04×10^{-6}

TABLE VI. Detailed components together with absolute values of the associated coefficients in the initial guess $\varphi_{0,2}$ (61) for group S2 in case of (70).

components of $\varphi_{0,2}$	dimensionless angular frequency ϵ								
(m^2/s)	1.0002	1.001	1.002	1.003	1.004	1.005	1.006	1.007	1.008
$\psi_{1,0}^2 \times 10^{-6}$	3.45	7.10	9.47	8.21	7.17	5.45	3.42	1.51	0.12
$\psi_{0,1}^2 \times 10^{-5}$	1.35	2.13	1.83	0.13	1.13	2.26	3.17	3.84	4.29
$\psi_{2,-1}^2 \times 10^{-6}$	0.54	1.36	2.09	2.56	2.87	2.99	2.95	2.84	2.70
$\psi_{3,-2}^2 \times 10^{-7}$	—	0.96	1.88	3.29	4.33	5.28	6.06	6.65	7.10
$\psi_{-1,2}^2 \times 10^{-4}$	—	0.51	1.13	1.89	2.11	2.17	2.10	1.95	1.77
$\psi_{4,-3}^2 \times 10^{-8}$	—	—	—	1.91	2.94	4.28	5.80	7.27	8.59
$\psi_{5,-4}^2 \times 10^{-9}$	—	—	—	0.16	0.36	1.00	2.09	3.41	4.75
$\psi_{-2,3}^2 \times 10^{-4}$	—	—	—	1.72	2.91	4.11	5.24	6.21	7.02

REFERENCES

Aghsaee, P., Boegman, L., and Lamb, K. G., "Breaking of shoaling internal solitary waves," Journal of Fluid Mechanics **659**, 289–317 (2010).

Aksel, N. and Schörner, M., "Films over topography: from creeping flow to linear stability, theory, and experiments, a review," Acta Mechanica **229**, 1453–1482 (2018).

Akylas, T. R. and Karimi, H. H., "Oblique collisions of internal wave beams and associated resonances," Journal of Fluid Mechanics **711**, 337–363 (2012).

Alam, M.-R., "A new triad resonance between co-propagating surface and interfacial waves," Journal of Fluid Mechanics **691**, 267–278 (2012).

Alam, M.-R., Liu, Y. M., and Yue, D. K. P., "Bragg resonance of waves in a two-layer fluid propagating over bottom ripples. Part I. Perturbation analysis," Journal of Fluid

Mechanics **624**, 191–224 (2009).

Alam, M.-R., Liu, Y. M., and Yue, D. K. P., "Oblique sub-and super-harmonic Bragg resonance of surface waves by bottom ripples," Journal of Fluid Mechanics **643**, 437–447 (2010).

Ball, F. K., "Energy transfer between external and internal gravity waves," Journal of Fluid Mechanics **19**, 465–478 (1964).

Benjamin, T. B., "Internal waves of finite amplitude and permanent form," Journal of Fluid Mechanics **25**, 241–270 (1966).

Benjamin, T. B., "Internal waves of permanent form in fluids of great depth," Journal of Fluid Mechanics **29**, 559–592 (1967).

Camassa, R., Rusas, P. O., Saxena, A., and Tiron, R., "Fully nonlinear periodic internal waves in a two-fluid system of finite depth," Journal of Fluid Mechanics **652**, 259–298 (2010).

Chen, M. J. and Forbes, L. K., "Steady periodic waves in a three-layer fluid with shear in the middle layer," Journal of Fluid Mechanics **594**, 157–181 (2008).

Dauxois, T., Joubaud, S., Odier, P., and Venaille, A., "Instabilities of internal gravity wave beams," Annual Review of Fluid Mechanics **50**, 131–156 (2018).

Fan, Z. S., Shi, X. G., Liu, A. K., Liu, H. L., and Li, P. L., "Effects of tidal currents on nonlinear internal solitary waves in the South China Sea," Journal of Ocean University of China **12**, 13–22 (2013).

Garrett, C. and Munk, W., "Space-time scales of internal waves: A progress report," Journal of Geophysical Research Atmospheres **80**, 291–297 (1975).

Garrett, C. and Munk, W., "Internal waves in the ocean," Annual review of fluid mechanics **11**, 339–369 (1979).

Grimshaw, R. and Helfrich, K., "The effect of rotation on internal solitary waves," IMA Journal of Applied Mathematics **77**, 326–339 (2012).

Grimshaw, R. H. J. and Smyth, N., "Resonant flow of a stratified fluid over topography," Journal of Fluid Mechanics **169**, 429–464 (1986).

Heining, C., Bontozoglou, V., Aksel, N., and Wierschem, A., "Nonlinear resonance in viscous films on inclined wavy planes," International Journal of Multiphase Flow **35**, 78–90 (2009).

Holyer, J. Y., "Large amplitude progressive interfacial waves," Journal of Fluid Mechanics **93**, 433–448 (1979).

Hunt, J. N., “Interfacial waves of finite amplitude,” La Houille Blanche **4**, 515–531 (1961).

Lake, B. M., Yuen, H. C., Rungaldier, H., and Ferguson, W. E., “Nonlinear deep-water waves: theory and experiment. part 2. evolution of a continuous wave train,” Journal of Fluid Mechanics **83**, 49–74 (1977).

Leonard, J. J. and Bahr, A., “Autonomous underwater vehicle navigation,” in *Springer Handbook of Ocean Engineering* (Springer, 2016) pp. 341–358.

Leonard, J. J., Bennett, A. A., Smith, C. M., and Feder, H. J. S., “Autonomous underwater vehicle navigation,” in *MIT Marine Robotics Laboratory Technical memorandum* (1998).

Liang, Y., Zareei, A., and Alam, M.-R., “Inherently unstable internal gravity waves due to resonant harmonic generation,” Journal of Fluid Mechanics **811**, 400–420 (2017).

Liao, S. J., *Beyond Perturbation: Introduction to the Homotopy Analysis Method* (CRC, Boca Raton, 2003).

Liao, S. J., *Homotopy Analysis Method in Nonlinear Differential Equations* (Springer-Verlag, New York, 2011).

Liao, S. J., “On the homotopy multiple-variable method and its applications in the interactions of nonlinear gravity waves,” Communications in Nonlinear Science and Numerical Simulation **16**, 1274–1303 (2011b).

Liao, S. J., Xu, D. L., and Stiassnie, M., “On the steady-state nearly resonant waves,” Journal of Fluid Mechanics **794**, 175–199 (2016).

Liu, Z. and Liao, S. J., “Steady-state resonance of multiple wave interactions in deep water,” Journal of Fluid Mechanics **742**, 664–700 (2014).

Liu, Z. and Xie, D., “Finite-amplitude steady-state wave groups with multiple near-resonances in finite water depth,” Journal of Fluid Mechanics **867**, 348–373 (2019).

Liu, Z., Xu, D. L., Li, J., Peng, T., Alsaedi, A., and Liao, S. J., “On the existence of steady-state resonant waves in experiments,” Journal of Fluid Mechanics **763**, 1–23 (2015).

Liu, Z., Xu, D. L., and Liao, S. J., “Mass, momentum, and energy flux conservation between linear and nonlinear steady-state wave groups,” Physics of Fluids **29**, 127104 (2017).

Liu, Z., Xu, D. L., and Liao, S. J., “Finite amplitude steady-state wave groups with multiple near resonances in deep water,” Journal of Fluid Mechanics **835**, 624–653 (2018).

Madsen, P. A. and Fuhrman, D. R., “Third-order theory for multi-directional irregular waves,” Journal of Fluid Mechanics **698**, 304–334 (2012).

Mccomas, C. H. and Bretherton, F. P., “Resonant interaction of oceanic internal waves,” Journal of Geophysical Research **82**, 1397–1412 (1977).

Okamura, M., "Almost limiting short-crested gravity waves in deep water," Journal of Fluid Mechanics **646**, 481–503 (2010).

Osborne, A. R. and Burch, T. L., "Internal solitons in the Andaman Sea," Science **208**, 451–460 (1980).

Parau, E. and Dias, F., "Interfacial periodic waves of permanent form with free-surface boundary conditions," Journal of Fluid Mechanics **437**, 325–336 (2001).

Phillips, O. M., "On the dynamics of unsteady gravity waves of finite amplitude. Part 1. The elementary interactions," Journal of Fluid Mechanics **9**, 193–217 (1960).

Ramp, S. R., Tang, T. Y., Duda, T. F., Lynch, J. F., Liu, A. K., Chiu, C. S., Bahr, F. L., Kim, H. R., and Yang, Y. J., "Internal solitons in the northeastern south china sea. part i: sources and deep water propagation," IEEE Journal of Oceanic Engineering **29**, 1157–1181 (2004).

Saffman, P. G. and Yuen, H. C., "Finite-amplitude interfacial waves in the presence of a current," Journal of Fluid Mechanics **123**, 459–476 (1982).

Schörner, M., Reck, D., and Aksel, N., "Does the topography's specific shape matter in general for the stability of film flows?" Physics of Fluids **27**, 042103 (2015).

Sutherland, B. R., *Internal gravity waves* (Cambridge university press, 2010).

Tadjbakhsh, I. and Keller, J. B., "Standing surface waves of finite amplitude," Journal of Fluid Mechanics **8**, 442–451 (1960).

Tanaka, M. and Wakayama, K., "A numerical study on the energy transfer from surface waves to interfacial waves in a two-layer fluid system," Journal of Fluid Mechanics **763**, 202–217 (2015).

Thorpe, S. A., "On wave interactions in a stratified fluid," Journal of Fluid Mechanics **24**, 737–751 (1966).

Tsai, C. P. and Jeng, D. S., "Numerical Fourier solutions of standing waves in finite water depth," Applied Ocean Research **16**, 185–193 (1994).

Vajravelu, K. and Van Gorder, R. A., *Nonlinear Flow Phenomena and Homotopy Analysis: Fluid Flow and Heat Transfer* (Springer-Verlag, Heidelberg, 2012).

Vanden-Broeck, J. M. and Schwartz, L. W., "Numerical calculation of standing waves in water of arbitrary uniform depth," The Physics of Fluids **24**, 812–815 (1981).

Wen, F., "Resonant generation of internal waves on the soft sea bed by a surface water wave," Physics of Fluids **7**, 1915–1922 (1995).

Wierschem, A., Bontozoglou, V., Heining, C., Uecker, H., and Aksel, N., "Linear resonance in viscous films on inclined wavy planes," International Journal of Multiphase Flow **34**, 580–589 (2008).

Xu, D. L., Lin, Z. L., Liao, S. J., and Stiassnie, M., "On the steady-state fully resonant progressive waves in water of finite depth," Journal of Fluid Mechanics **710**, 379–418 (2012).

Yang, X. Y., Dias, F., and Liao, S. J., "On the steady-state resonant acoustic-gravity waves," Journal of Fluid Mechanics **849**, 111–135 (2018).

Zaleski, J., Zaleski, P., and Lvov, Y. V., "Excitation of interfacial waves via surface-interfacial wave interactions," arXiv preprint arXiv:1904.08329 (2019).

Zhang, H. P., King, B., and Swinney, H. L., "Resonant generation of internal waves on a model continental slope," Physical Review Letters **100**, 244504 (2008).

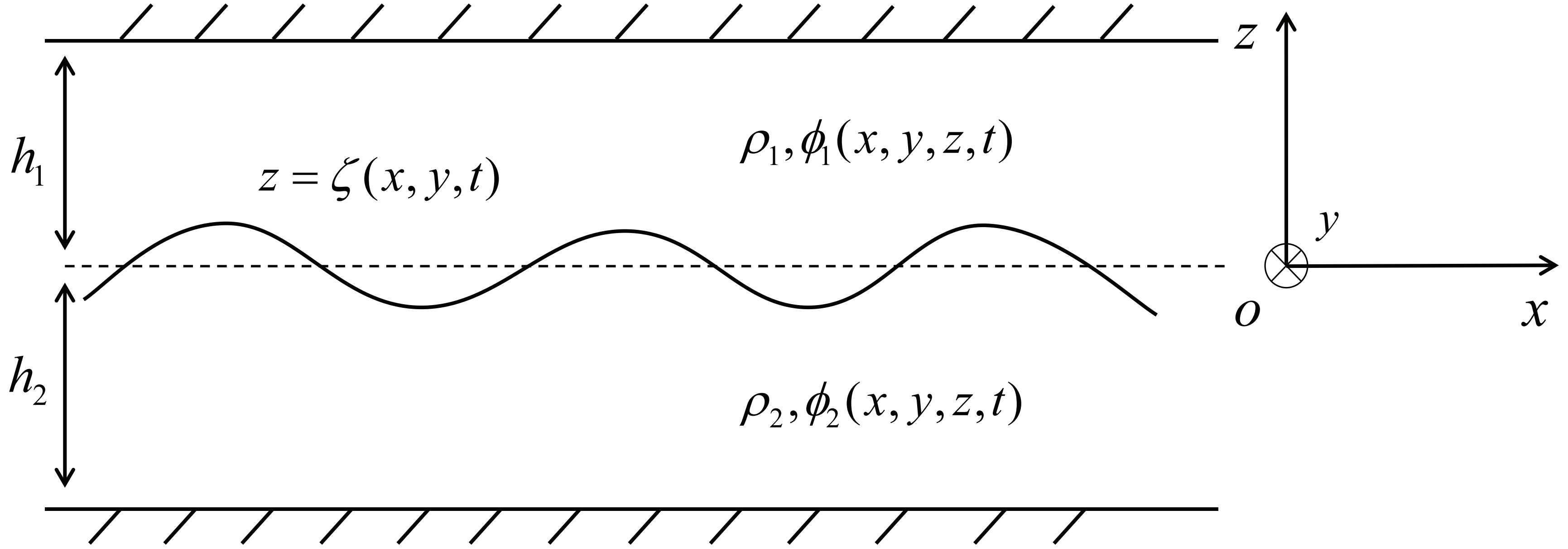

z
h_1
$\rho_1, \phi_1(x, y, z, t)$
$z = \zeta(x, y, t)$
y
o
x
h_2
$\rho_2, \phi_2(x, y, z, t)$

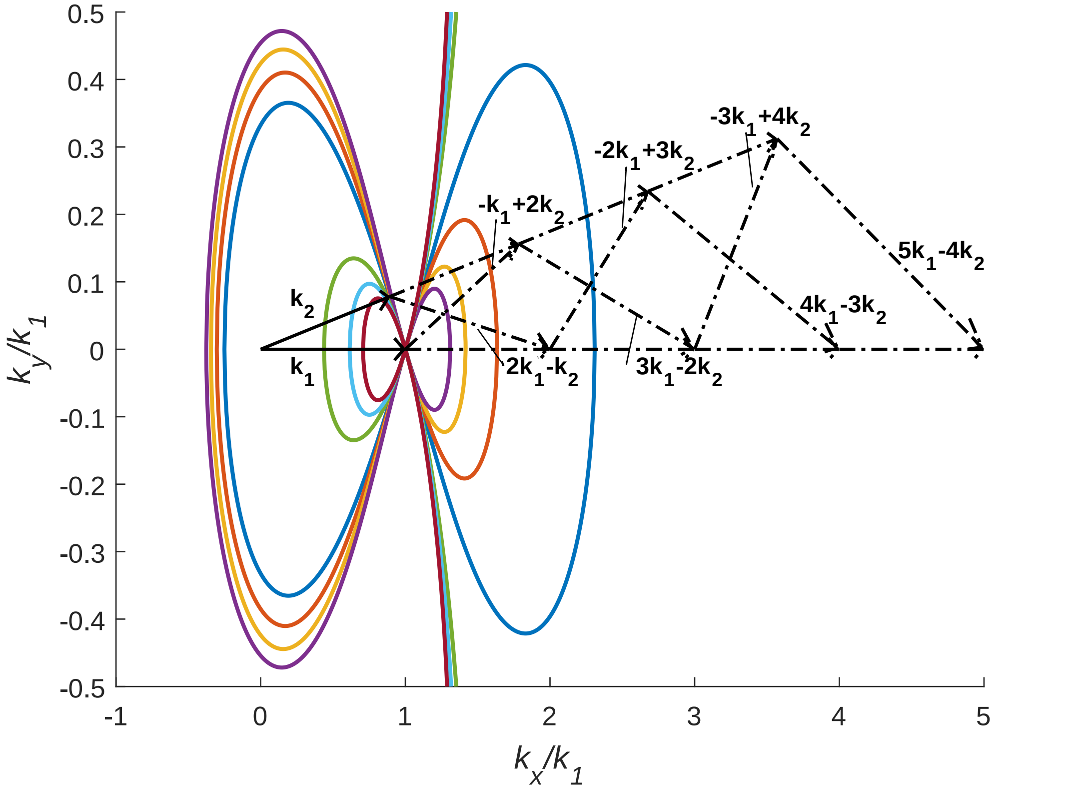

0.5
0.4
0.3
0.2
0.1
0
-0.1
-0.2
-0.3
-0.4
-0.5
k_y/k_1
-1
0
1
2
3
4
5
k_x/k_1
k_2
k_1
$-k_1+2k_2$
$-2k_1+3k_2$
$-3k_1+4k_2$
$2k_1-k_2$
$3k_1-2k_2$
$4k_1-3k_2$
$5k_1-4k_2$

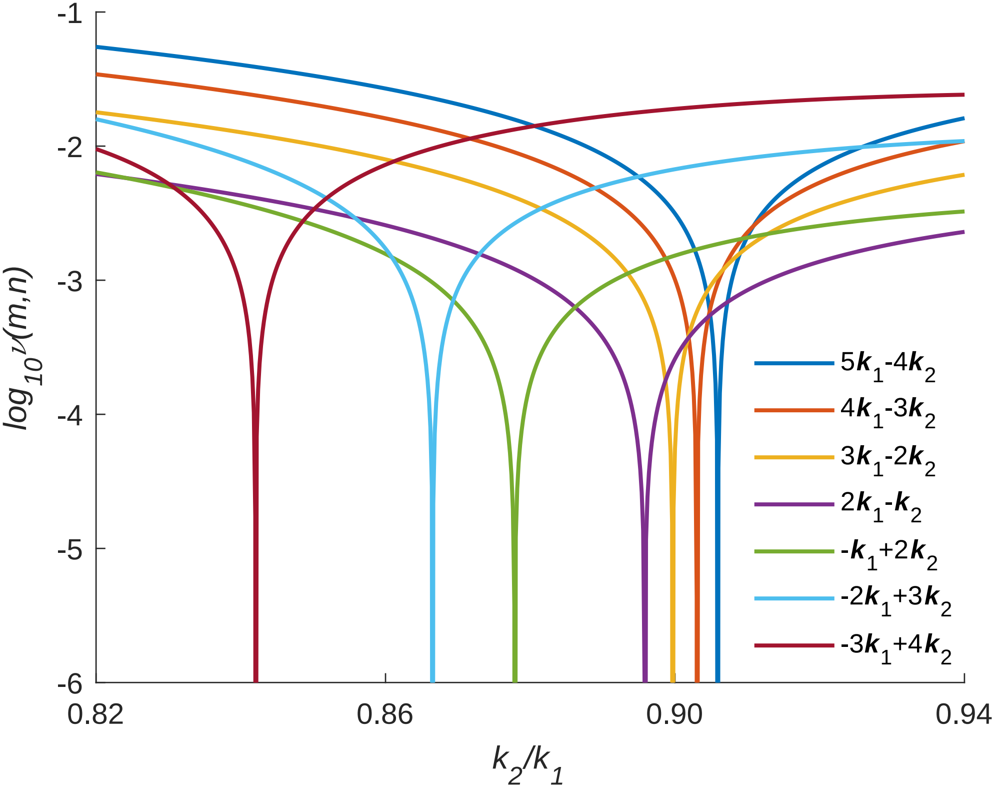

-1
-2
-3
-4
-5
-6
0.82
0.86
0.90
0.94
$log_{10} \nu(m,n)$
k_2/k_1
5$\boldsymbol{k}_1$-4$\boldsymbol{k}_2$
4$\boldsymbol{k}_1$-3$\boldsymbol{k}_2$
3$\boldsymbol{k}_1$-2$\boldsymbol{k}_2$
2$\boldsymbol{k}_1$-$\boldsymbol{k}_2$
-$\boldsymbol{k}_1$+2$\boldsymbol{k}_2$
-2$\boldsymbol{k}_1$+3$\boldsymbol{k}_2$
-3$\boldsymbol{k}_1$+4$\boldsymbol{k}_2$

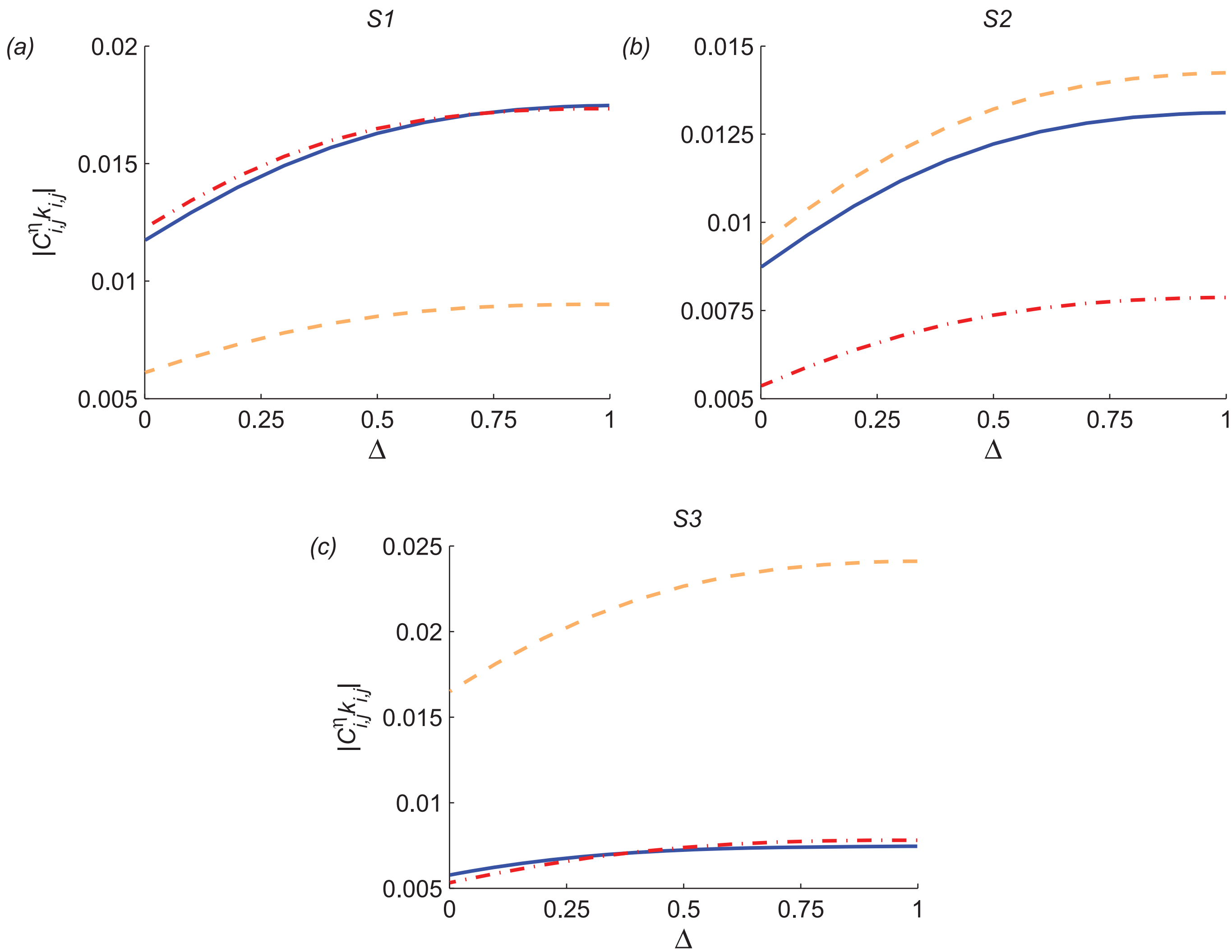
(a)
S1
0.02
0.015
0.01
0.005
|C^η_{i,j} k_{i,j}|
0
0.25
0.5
0.75
1
Δ
(b)
S2
0.015
0.0125
0.01
0.0075
0.005
0
0.25
0.5
0.75
1
Δ
(c)
S3
0.025
0.02
0.015
0.01
0.005
|C^η_{i,j} k_{i,j}|
0
0.25
0.5
0.75
1
Δ

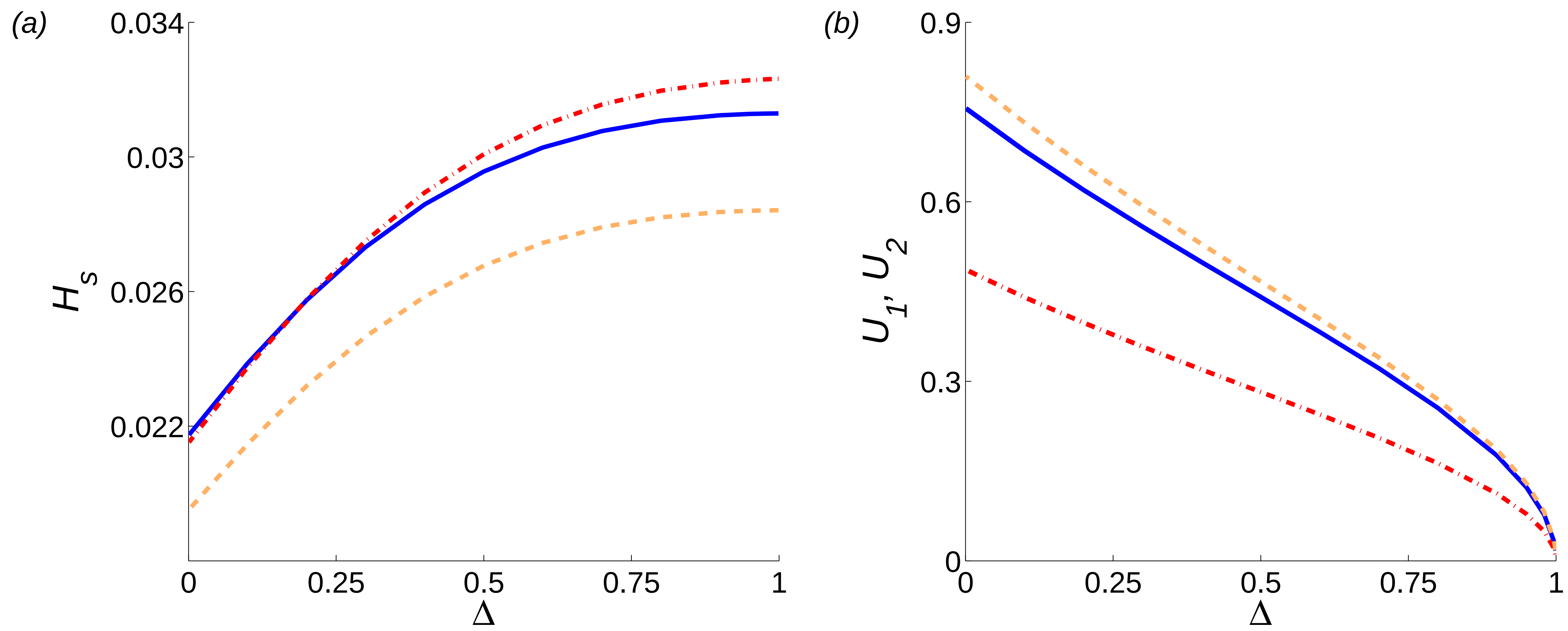
(a)
0.034
0.03
0.026
0.022
H_s
0
0.25
0.5
0.75
1
Δ
(b)
0.9
0.6
0.3
0
U_1, U_2
0
0.25
0.5
0.75
1
Δ

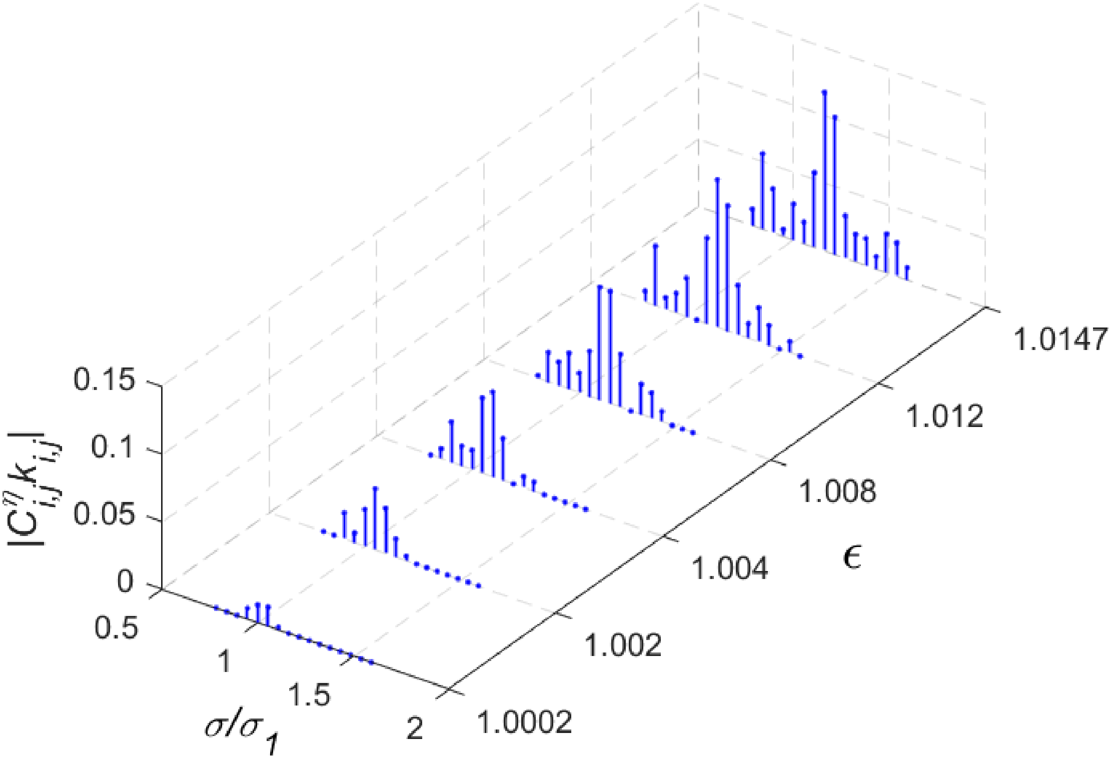
0.15
0.1
0.05
0
$|C^{\eta}_{i,j} k_{i,j}|$
0.5
1
1.5
2
σ/σ_1
1.0002
1.002
1.004
1.008
1.012
1.0147
ϵ

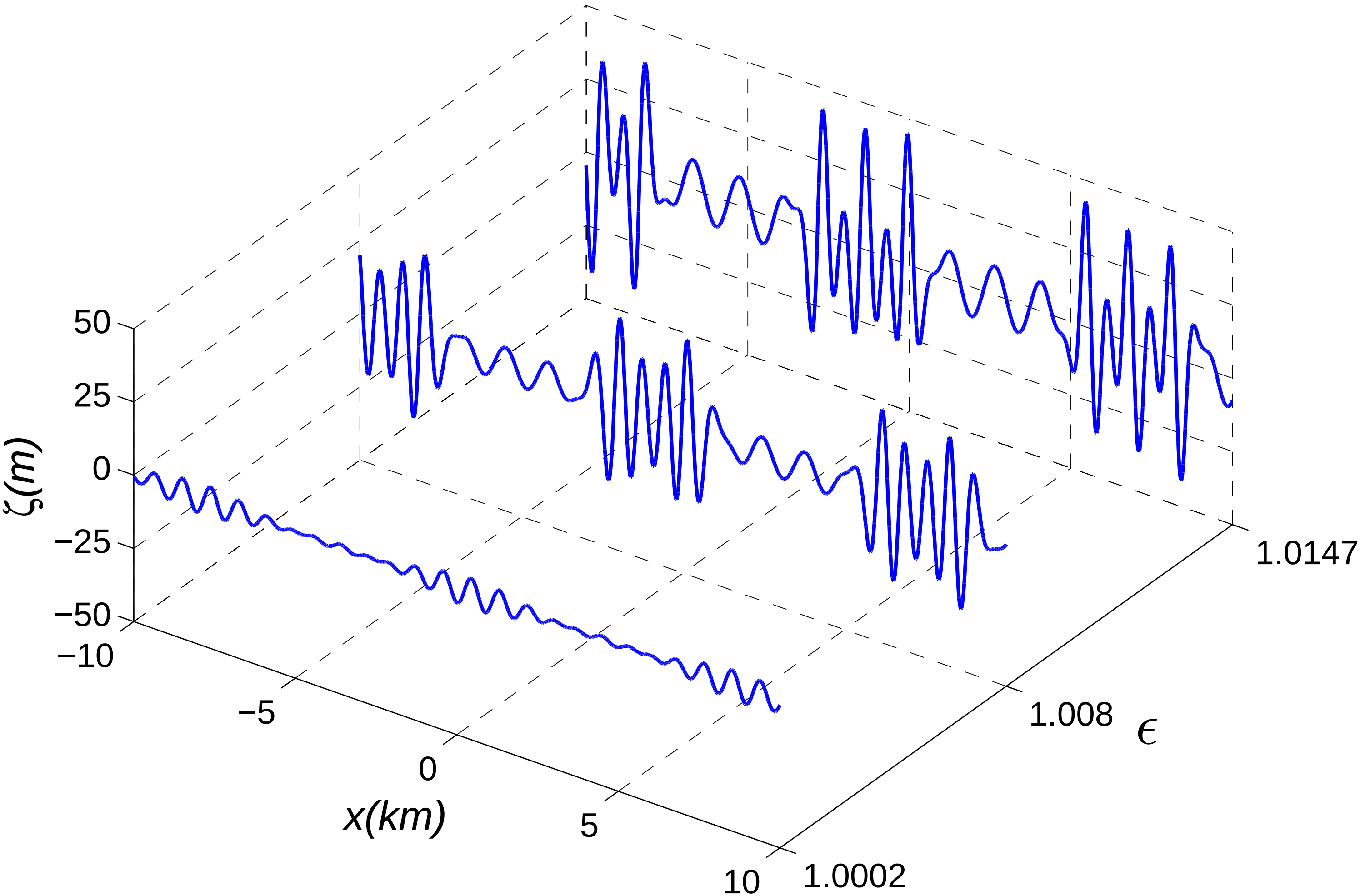

50
25
0
−25
−50
ζ(m)
−10
−5
0
5
10
x(km)
1.0002
1.008
1.0147
ϵ

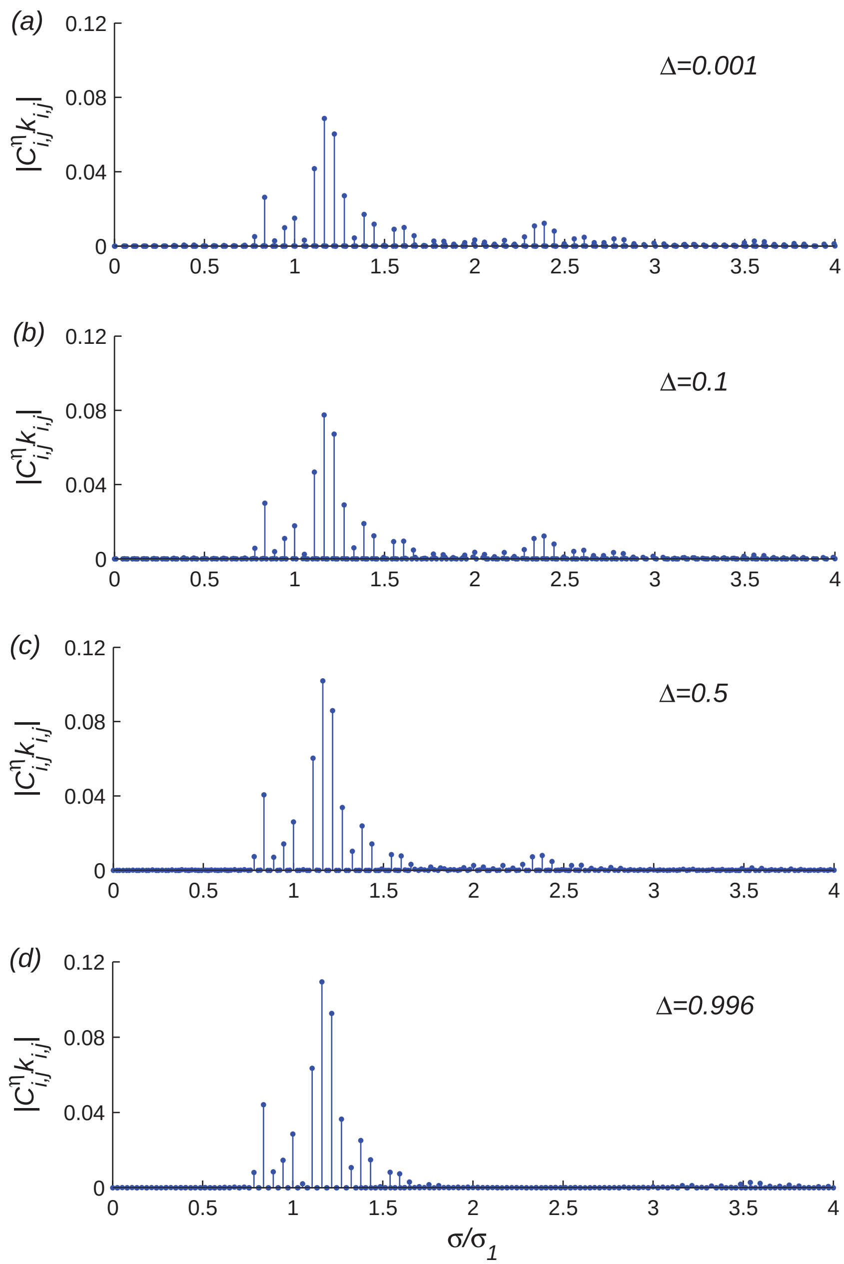
(a)
Δ=0.001
(b)
Δ=0.1
(c)
Δ=0.5
(d)
Δ=0.996
|C^η_{i,j} k_{i,j}|
0.12
0.08
0.04
0
0.5
1
1.5
2
2.5
3
3.5
4
σ/σ_1

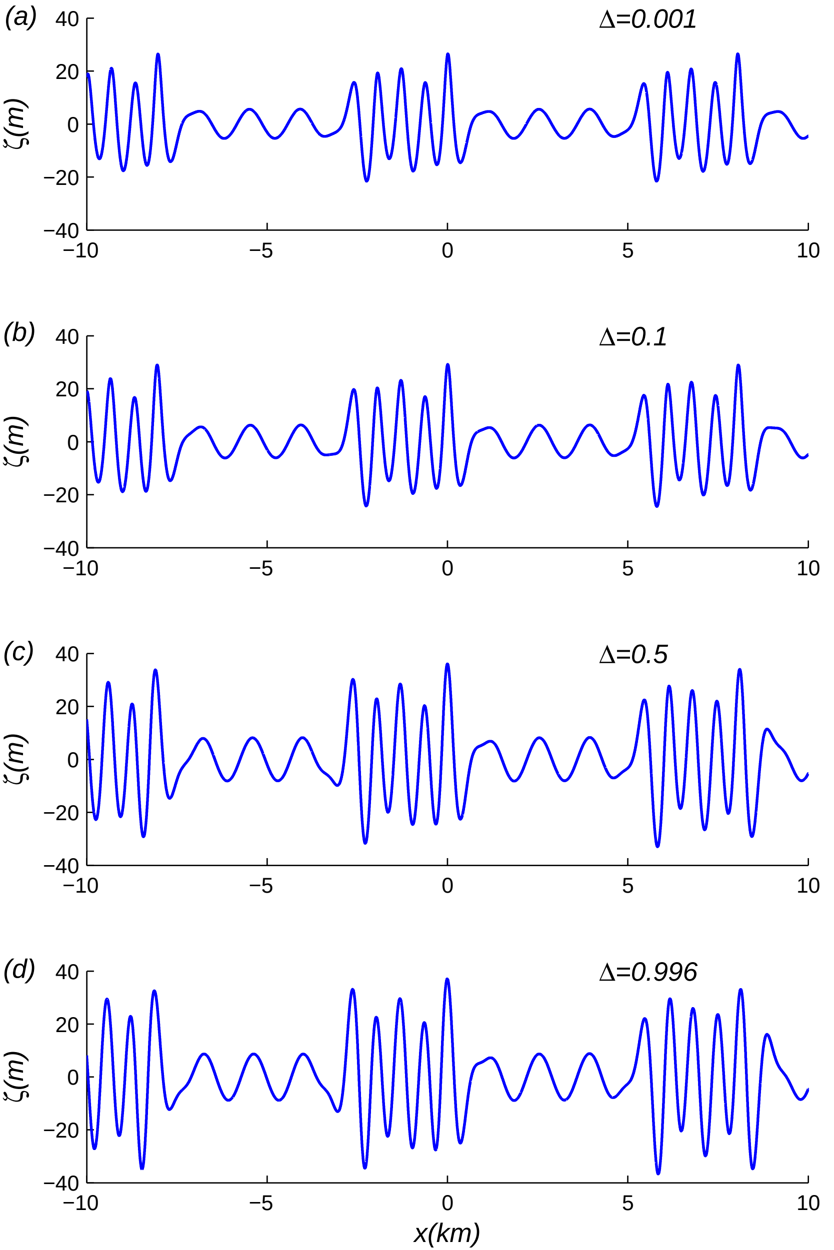
(a)
Δ=0.001
(b)
Δ=0.1
(c)
Δ=0.5
(d)
Δ=0.996
ζ(m)
40
20
0
−20
−40
−10
−5
0
5
10
x(km)

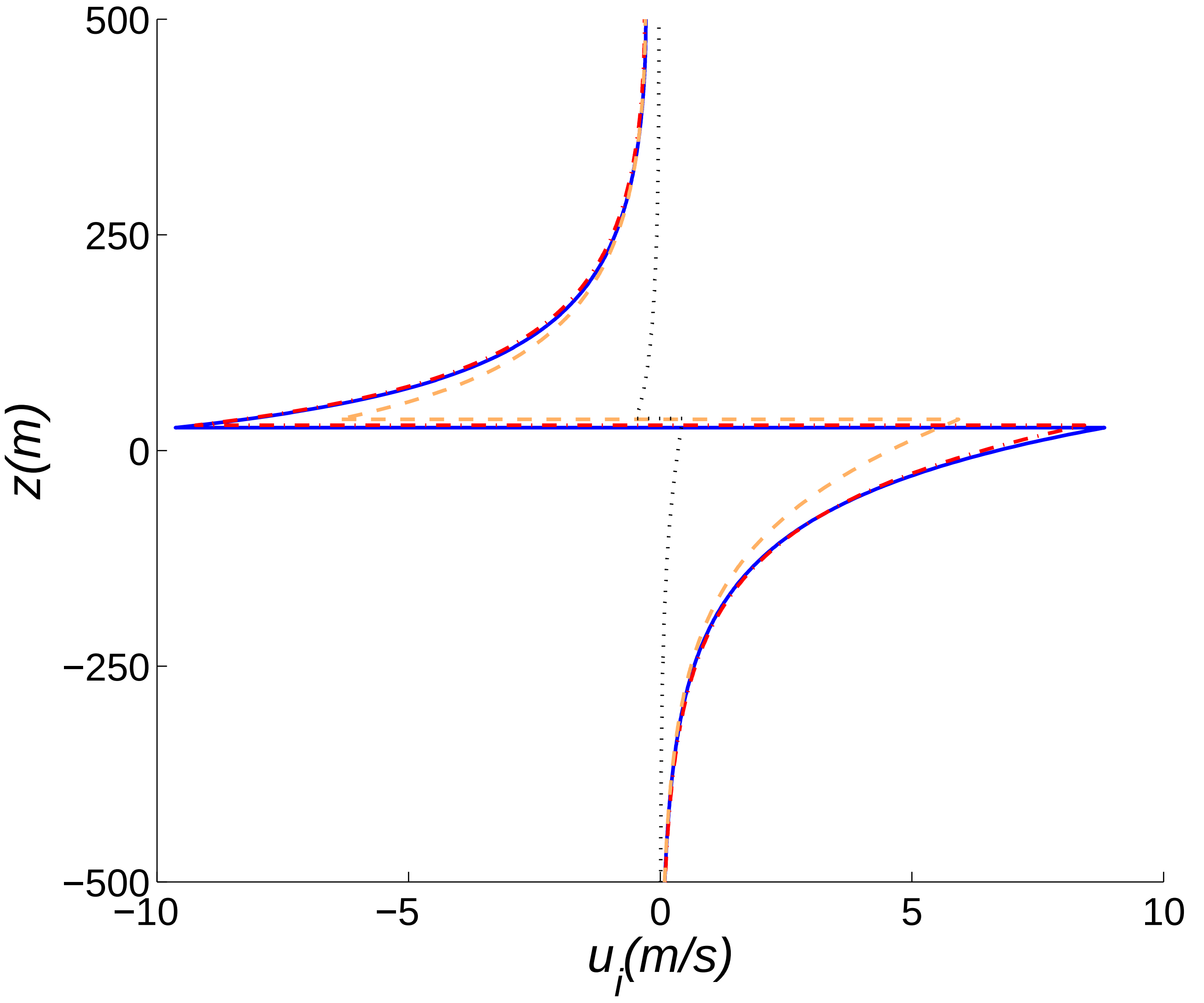

500
250
0
−250
−500
z(m)
−10
−5
0
5
10
u_i(m/s)